RSC Advances

REVIEW

View Article Online
View Journal | View Issue

Cite this: *RSC Adv.*, 2025, **15**, 35807

Antimicrobial activity of chitosan, alginate, pectin, and cellulose-based biopolymer composites with silver, copper oxide, and zinc oxide nanoparticles

Roxana Yesenia Pastrana-Alta,[a] Emily Huarote-Garcia,[b] Miguel Adolfo Egusquiza-Huamani[a] and Angélica M. Baena-Moncada*[c]

Received 16th March 2025
Accepted 4th September 2025

DOI: 10.1039/d5ra01892g

rsc.li/rsc-advances

Nanotechnology has revolutionized materials science, particularly through the incorporation of metallic nanoparticles into biopolymers, enhancing their physicochemical, mechanical, and biological properties for diverse applications. Polysaccharide-based biopolymers, such as chitosan, alginate, pectin, and cellulose, play a crucial role in antimicrobial applications due to their unique structural and functional properties. Their combination with metallic nanoparticles further enhances their antimicrobial effectiveness, making them promising materials for biomedical, environmental, and food applications. However, their inherent limitations, including poor mechanical strength and high permeability, necessitate functional modifications. The integration of metallic or metallic oxide nanoparticles (NPs), such as silver (AgNPs), copper oxide (CuONPs), and zinc oxide (ZnONPs), has shown remarkable improvements in antimicrobial activity, thermal stability, and mechanical performance. Green synthesis approaches utilizing plant extracts, microbial processes, and bio-waste have emerged as sustainable alternatives to conventional chemical methods, reducing environmental impact while enhancing NP

[a]*BIOMET Laboratorio de Química Bioinorgánica en Medicina, Medioambiente y Tecnología, Facultad de Ciencias de la Universidad Nacional de Ingeniería, Av. Túpac Amaru 210, Rímac, Lima, Peru*

[b]*Laboratorio de Productos Naturales, Departamento de Química, Facultad de Ciencias, Universidad de Chile, Las Palmeras 3425, 7800024 Santiago, Chile*

[c]*Laboratorio de Investigación de Electroquímica Aplicada, Facultad de Ciencias de la Universidad Nacional de Ingeniería, Av. Túpac Amaru 210, Rímac, Lima, Peru. E-mail: abaenam@uni.edu.pe*

Roxana Yesenia Pastrana Alta

Roxana Yesenia Pastrana Alta is a Chemistry professor at the National University of Engineering (UNI), Lima, Peru, and leads the Bioinorganic Chemistry in Medicine, Environment, and Technology (BIOMET) research group. A member of the College of Chemists of Peru, she graduated in Chemistry from UNI in 2010 and earned her PhD in Chemistry from the University of São Paulo, Brazil, in 2016. Her research specializes in developing biopolymeric materials from biomass residues through automated processes, with applications in medicine, water treatment, synthetic chemistry, and peptide engineering, including treatments for iron overload and tuberculosis. She also investigates the ecotoxicology of advanced materials using bioindicators like Daphnia magna and Artemia salina, focusing on sustainable and innovative solutions in science and technology.

Emily Huarote-Garcia

Emily G. Huarote Garcia is a student in the PhD program in Chemistry at the University of Chile, Santiago, Chile. She graduated in Chemistry from the National University Federico Villarreal in Peru in 2016 and received her Master's degree from the National University of Engineering in 2023. She is a member of the Chemical Society of Peru. Her research focuses on the field of natural products and green chemistry. She is also interested in the development of new green methodologies for the synthesis of nanomaterials and the separation of organic compounds.

stability and biocompatibility. This review provides a comprehensive analysis of the synthesis, characterization, and functionalization of polysaccharide-based biopolymer–nanoparticle composites, highlighting their advantages, challenges, and diverse applications. The development of these multifunctional materials offers promising solutions for critical challenges in healthcare, environmental sustainability, and food safety. Future research should focus on optimizing large-scale production, ensuring nanoparticle safety, and expanding the applications of biopolymer–nanoparticle composites through innovative synthesis and crosslinking techniques.

1. Introduction

The growing demand for sustainable and functional materials has catalyzed extensive research into carbohydrate-based biopolymers, particularly polysaccharides such as chitosan, alginate, pectin, and cellulose. These polysaccharides exhibit unique structural and functional properties that enable their interaction with metallic nanoparticles, leading to enhanced antimicrobial performance. These biopolymers, defined as polymeric materials based on polysaccharides such as alginate, chitosan, pectin, cellulose, starch, and lignin, exhibit favorable properties such as biocompatibility, biodegradability, low immunogenicity, and non-toxicity.[1–5] Derived from natural sources, including marine algae (*e.g.*, *Laminaria*, *Fucus*), crustacean exoskeletons (*e.g.*, shrimp, crab), fungi (*e.g.*, *Aspergillus niger*), and terrestrial plants and crops (*e.g.*, corn, wheat, potato, cassava, apple, citrus fruits), these materials offer versatility and a wide range of applications across industries. Biopolymers can be classified into natural or semi-synthetic categories, as illustrated in classification schemes such as those described by Baranwal *et al.*[6] Despite their advantageous properties, biopolymers face intrinsic limitations, including poor mechanical strength, susceptibility to microbial degradation, and in some cases, high permeability to gases or water vapor, which can compromise their barrier properties in packaging or biomedical applications.[7–9]

Among biopolymers, chitosan and alginate hold prominent positions due to their unique properties and diverse applications. Chitosan, a derivative of chitin obtained through deacetylation, is abundant in the exoskeletons of crustaceans and the cell walls of fungi. Its structure, featuring primary amine and hydroxyl groups, allows for chemical modification without altering its degree of polymerization. Chitosan has demonstrated excellent antimicrobial properties against both Gram-positive and Gram-negative bacteria, which depend primarily on its molecular weight and degree of deacetylation (DD) (Table 1). This cationic polysaccharide disrupts microbial cell membranes through electrostatic interactions, making it a highly effective material for antimicrobial applications.[10] Its low toxicity, biodegradability, and biocompatibility make chitosan an ideal candidate for biomedical uses, including wound dressings, surgical sutures, drug and gene delivery systems, and artificial tissue scaffolds.[11] Furthermore, chitosan's versatility extends to its use as a matrix for nanoparticles, enhancing properties such as mechanical strength, wettability, tear resistance, tensile strength, and elongation capacity, critical for

Miguel Adolfo Egusquiza Huamani

Miguel Adolfo Egusquiza Huamani is an undergraduate student of Chemistry at the National University of Engineering (UNI), Lima, Perú. He is an active member of the Bioinorganic Chemistry in Medicine, Environment and Technology (BIOMET) research group and a founder member of the UNI ACS Student Chapter. His research focuses on the transformation of biomass wastes into advanced biopolymers designed for high impact applications in environmental applications, specifically in the removal of metallic contaminants in aqueous systems, and their biological properties against fungal organisms and bioindicators.

Angélica M. Baena-Moncada

Angélica M. Baena-Moncada is an Associate Professor at the National University of Engineering, Lima, Peru. She is also a member of the Research Group of Applied Electrochemistry and the Accreditation Committee of the School of Chemistry of the Faculty of Sciences at the same institution. She graduated in Chemistry from the University of Quindío in Colombia in 2010 and received her PhD from the National University of Río Cuarto in Argentina in 2015. Her research focuses on developing carbonaceous materials from biomass waste, with applications in supercapacitors and sensors, and as support for nanoelectrocatalysts for fuel cell applications. She is also interested in the fabrication of nanomaterial-based sensors and the synthesis of hierarchical materials for hydrogen production and microbial fuel cells. In 2024, she was honored with the Latin Woman of Impact award. She is a member of the Peruvian Electrochemical Society.

Table 1 Sources, extraction methods, physicochemical properties and characterization of chitosan obtained on current research

Sources	Species	Extraction methods	Molecular weight (kDa)	Deacetylation degree (%)	Key characteristics	Ref.
Deep-sea mud shrimp	*Solenocera hextii*	Chemical extraction	263.95	75.5	High water and fat binding capacity	16
Snail shell	*Archachatina marginata*	Chemical extraction	220	94.71	High removal of methylene blue	17
Pink shrimp shell	*Parapenaeus longirostris*	Chemical extraction	310	81.50	Smooth surface and nanofiber structure	18
Insect exoskeleton	*Hermetia illucens*	Chemical extraction	35	90	Crystallite size 3 nm, and good film capacity	19
Cockroach exoskeleton	*Eupolyphaga sinensis*	Chemical extraction	127.79	96.57	Antibacterial nanofiber	20
Fish	*Prochilodus magdalenae*	Chemical extraction	107.18–240.3	94.91	High viscosity and antibacterial effect	21
Shrimp shell	—	Chemical extraction	280	88.2	Adsorbent microsphere	22
Crayfish shell	*Parastacus pugnax*	Chemical extraction	589.43	91.55	Antimicrobial and antioxidant activity	23
Shrimp shell	*Litopenaeus vannamei*	Biological extraction	246.4	74.9	High antioxidant and antibacterial activity	24
Shrimp shell	—	Biological extraction	144	86.2	Antioxidant and antimicrobial activity	25
Shrimp shell	*Litopenaeus vannamei*	Biological extraction	71.31	78	Low deacetylation degree	26
Shrimp shell	*Penaeus vannamei*	Biological extraction	394.52	90.75	Improvement in viscosity and solubility	27
Shrimp shell	—	Ultrasonic extraction	4.94	87.73	Green process	28
Shrimp shell	—	Ultrasound extraction	55.66	94.03	Low particle size	29
Shrimp shell	*Metapenaeus monoceros*	Microwave extraction	14.125	86.7	Low crystallinity, low viscosity	30

applications like tissue engineering and advanced wound healing.[12–15]

Alginate, another polysaccharide biopolymer, is primarily sourced from brown algae or microbial cultures and is composed of β-D-mannuronate and α-L-guluronate blocks. Its gel-forming capabilities, biocompatibility, biodegradability, and lack of immunogenicity make alginate an invaluable material for a wide array of biomedical applications. These include tissue engineering scaffolds, controlled drug release systems, wound dressings, and 3D bioprinting, among others.[31,32] Beyond biomedicine, alginate finds extensive applications in biotechnology, packaging, aquaculture, cosmetics, and the food industry, underscoring its versatility. Its ability to form hydrogels under mild conditions has been exploited in regenerative medicine for promoting tissue healing and re-epithelialization.[33]

To address the limitations of unmodified biopolymers, researchers have turned to nanotechnology. Nanoparticles exhibit an exceptionally high surface area-to-volume ratio, meaning that a substantial proportion of their atoms or molecules are located at the surface, where they can participate in chemical, physical, or biological interactions. This property is critical for enhancing reactivity, catalytic efficiency, and interfacial bonding when incorporated into polymeric matrices.[34,35] In biopolymer-based nanocomposites, nanoparticles can be integrated *via* various approaches, including doping, alloying, heterostructure fabrication, core–shell architecture, cluster formation, or *in situ* synthesis, each offering distinct advantages in nanoparticle dispersion, interface stability, and functional performance.[36] Nanoparticles such as AgNPs, CuONPs, and ZnONPs exhibit unique properties, including high surface area, potent antimicrobial activity, and catalytic functions. When incorporated into biopolymer matrices, these nanoparticles form nanocomposites with enhanced mechanical, thermal, and antimicrobial properties.[37] For instance, chitosan–AgNP nanocomposites synthesized using green methods, such as tea polyphenols as reducing agents, have demonstrated potent antibacterial activity against pathogens like *Escherichia coli* and *Staphylococcus aureus*.[38,39] Similarly, alginate-based nanocomposites with nanoparticles like CuONPs and ZnONPs have shown improved food preservation properties, extended shelf life and mitigating fungal contamination.[25] The synergistic integration of biopolymers and NPs is not limited to biomedical applications. In environmental contexts, nanocomposites such as graphene oxide-chitosan with iron oxide nanoparticles have shown exceptional heavy metal adsorption capacities for water purification, offering a sustainable solution for addressing pollution.[37,40] Green synthesis methods have gained prominence for producing these materials, emphasizing the reduction of toxic reagents and the incorporation of plant-derived compounds as stabilizing and reducing agents.[41]

This review provides a comprehensive analysis of recent advancements in biopolymer–nanoparticle composites, with a focus on their synthesis, characterization, and diverse applications as antimicrobial materials. By evaluating their benefits, limitations, and prospects, this work seeks to illuminate the potential of these multifunctional materials in addressing critical challenges in healthcare, environmental protection, and food safety.

2. Review methodology

A systematic literature review was conducted to evaluate scientific research on the synthesis of modified and unmodified polymer composites, as well as their various applications. The inclusion criteria focused on peer-reviewed journal articles and review articles published in English between 2018 and 2024. Conference proceedings and thesis were excluded from the

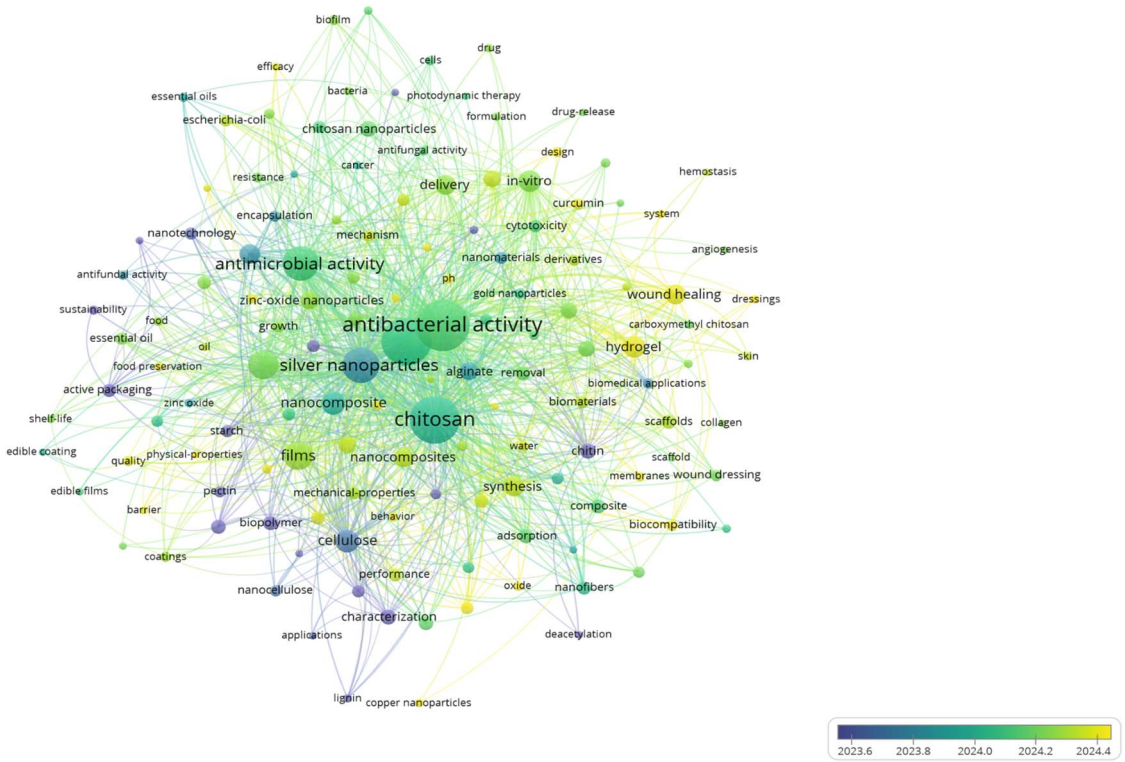

Fig. 1 Keyword co-occurrence map of publications related to antimicrobial activity of polysaccharide-based biopolymer–nanoparticle composites (2015–2024), generated with VOSviewer.

analysis. The literature search was conducted using scientific databases such as Elsevier (Web of Science), SpringerLink, Scientific Reports, and other indexed sources. The following search query was used to retrieve relevant publications:

TS = (antimicrobial OR antibacteria* OR antifungal*) AND (polysaccharide* OR biopolymer* OR chitosan OR alginate OR cellulose) AND (nanoparticle* OR nanocomposite* OR AgNP* OR ZnO) AND PY = (2018–2024) AND DT = (Article OR Review OR Book OR Book Chapter).*

Articles that met the inclusion criteria were exported and analyzed using VOSviewer 1.6.20 (**https://www.vosviewer.com**, accessed June 10, 2025). Bibliometric mapping allowed for the extraction and visualization of metadata, including co-occurring keywords, publication sources, and citation networks. In the resulting maps, node size represents the relative importance of keywords, while node proximity reflects the strength of the association between terms, as shown in Fig. 1.

3. Synthesis and characterization of biopolymers

3.1. Chitosan

Chitosan (CS) is a cationic polysaccharide derived from the deacetylation of chitin, which is the second most abundant biopolymer in nature.[28] It consists of β-(1 → 4)-2-acetamido-D-glucose and β-(1 → 4)-2-amido-D-glucose units, with the latter being predominant, comprising approximately 70% of its structure.[18] This biopolymer is primarily isolated from the exoskeleton of various crustaceans, such as shrimp, crab, krill and crayfish.[23,42–44] CS can also be obtained from alternative sources, including the exoskeleton of insects, mollusk shells, fish scales and certain fungi.[17,21,32,45] CS is a highly versatile polysaccharide due to the reactivity of the functional groups (–OH and $–NH_2$) distributed along its polymeric chain, enabling interactions with a broad range of molecules, ions, metal surfaces, and cell membranes.[46] Due to its modified carbohydrate structure, CS exhibits distinct properties such as non-toxicity, antimicrobial activity, and antioxidant capacity.[47] CS is widely recognized for its extensive applications in the pharmaceutical, biomedical, and food industries, attributed to its biodegradability, biocompatibility, and excellent antibacterial, antifungal, and antioxidant properties (Table 1).[20,48]

3.1.1. Chitosan extraction methods. The extraction of CS from natural resources begins with a demineralization process aimed at removing inorganic salts, such as calcium carbonate ($CaCO_3$) present in the raw material.[19] This step typically employs strong acids, including hydrochloric acid (HCl) and sulfuric acid (H_2SO_4). However, recent investigations have focused on more sustainable alternatives, such as acetic acid (CH_3COOH), providing an eco-friendly approach.[49] The subsequent deproteinization step eliminates proteins associated with chitin, usually through alkaline treatment with sodium hydroxide (NaOH). In certain cases, a bleaching process is performed to remove residual pigments using oxidizing agents such as hydrogen peroxide (H_2O_2) and sodium hypochlorite (NaClO), or organic solvents like acetone (CH_3COCH_3),

depending on the characteristic of the raw material.[50,51] The final step, deacetylation hydrolyzes the acetamide groups (–$NHCOOCH_3$) present in chitin in a highly alkaline medium.[52] Fig. 2a shows a general extraction of CS from the exoskeleton of a crustacean involving steps previously mentioned. Key parameters, such as temperature, base concentration, and particle size, significantly influence the DD,[16] a critical factor affecting chitosan's solubility, viscosity, crystallinity, hydrophobicity, and biological activity.[24,53]

The biological extraction of CS represents a sustainable alternative to traditional chemical methods, which typically involve extreme temperature conditions and aggressive chemical agents such as HCl and NaOH.[24] Previous works highlighted that this method takes advantage of enzymes and microorganisms, such as bacteria and fungi, to decompose the raw material catalyze the deacetylation and degradation of chitin under mild conditions.[25] Thus, reducing the environmental impact and increasing the efficiency of CS extraction and its industrial applications. The use of proteases as biological tools during the deproteinization stage has proven to be highly efficient in preserving the natural structure of chitin, obtaining CS with DD higher than 90%.[27]

The application of ultrasound and microwave technology in the CS extraction has emerged as an eco-friendly alternative to traditional methods that produce hazardous waste, limiting the sustainability of the process.[54] Ultrasonic irradiation uses high frequency waves to generate microbubbles that collapse and release thermal and mechanical energy significantly improving the CS extraction.[29] Previous studies have confirmed that this method reduces reaction time, minimizes reagent consumption and temperature, while at the same time improving its physicochemical properties.

In recent years, various strategies have been developed to optimize the extraction of CS, since the traditional extraction method presents drawbacks due to prolonged reaction times, high energy consumption, and the use of hazardous chemical reagents.[55] Among these approaches, microwave-assisted extraction has emerged as a highly efficient technique, enabling the direct transfer of energy to the raw material's surface, thereby markedly reducing both extraction time and solvent usage.[56] Moreover, this method is characterized by lower energy consumption and shorter reaction durations while also improving the chemical properties of CS. Due to these advantages, microwave-assisted extraction has gained recognition as a sustainable and efficient alternative for CS extraction.[57] The study of Erwais *et al.* reported that applying microwaves at power levels of 875 and 1250 W for reaction times of 10, 15, and 20 min resulted in CS with a high DD (86.7%). However, this method also yielded CS with a low MW (14.125 kDa) and crystallinity index (46.57%).[30]

3.1.2. Characterization of the extracted chitosan. Rasweefali *et al.* evaluated the effect of deacetylation time on the properties of CS derived from deep-sea mud shrimp (*Solenocera hextii*). The chemical extraction involved demineralization with 1 mol L^{-1} HCl at room temperature for 1 h and deproteinization with 1 mol L^{-1} NaOH at 90 °C for 1 h. During deacetylation, a 45% NaOH solution at 100 °C was applied, varying reaction times to 1.5, 3.0 and 6.0 h (CS-1.5, CS-3.0 and CS-6.0). The DD

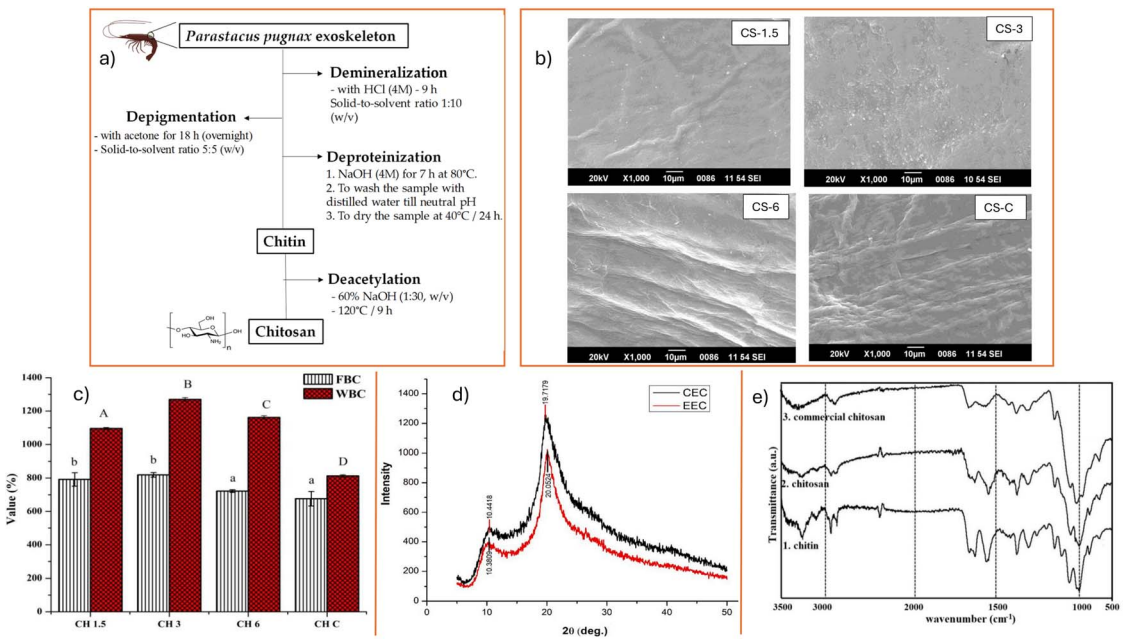

Fig. 2 (a) General chitosan extraction process from crustacean exoskeleton (*Parastacus pugnax*) reproduced from ref. 23 copyright © 2021 under the terms and conditions of CC BY license; (b) SEM images showing the surface morphology of chitosan due to the effect of deacetylation time; (c) FBC and WBC of extracted chitosan from deep-sea mud shrimp. Reproduced with permission from ref. 16 copyright © 2021 Elsevier Ltd. All rights reserved; (d) XRD of chemically extracted chitosan (CEC) and enzymatic extracted chitosan (EEC) reproduced with permission from ref. 3 copyright © 2023 Elsevier B.V. All rights reserved. (e) Comparison of FTIR spectra of commercial chitosan, ultrasonically extracted chitosan, and chitin reproduce from ref. 28 copyright © 2021 Elsevier Ltd. All rights reserved.

increased with reaction time, reaching 75.5 (CS-1.5), 85 (CS-3), and 87% (CS-6). Scanning electron microscopy (SEM) analysis (Fig. 2b) revealed changes in surface morphology, with reduced porosity, and increased smoothness, closely resemble commercial chitosan (CS-C). Fig. 2c shows that in both analyses of water binding capacity (WBC) and fat binding capacity (FBC), the CS extracted from deep-sea mud shrimp presented higher values compared to commercial chitosan (WBC: 812.67, FBC: 676.2%), being CS-3 the one with the highest values (WBC: 1270, FBC: 819.17%), making it suitable for food and medicinal applications.[16]

Recent studies that have varied the parameters of the deacetylation process have reported the successful production of CS with enhanced antimicrobial and antioxidant properties.[20] For instance, Ramirez *et al.* investigated the effect of different NaOH concentrations (2, 4 and 6 wt%) during the extraction of chitin from fish scale (*Prochilodus magdalenae*). They reported an exceptionally high DD (94.91, 100.06 and 100.99%), accompanied by a significant increase in bactericidal activity against *Staphylococcus aureus* and *Escherichia coli*, compared to commercial CS. This behavior was attributed to its low molecular weight (MW) of 107.18 kDa, which facilitates penetration through bacterial cell walls. Fourier transform infrared spectroscopy (FTIR) analysis revealed a decrease in the intensity of the –OH band in the extracted CS, which is associated with the presence of intermolecular hydrogen bonds characteristic of the β-chitosan structure. Furthermore, SEM images show a fibrillar structure for the 2 wt% NaOH-treated CS exhibiting a less smooth surface. These results highlight fish waste as a promising source for CS production with a high degree of deacetylation, low molecular weight and improved bactericidal property, expanding its potential in biomedical and environmental applications.

In the work by Cesar Burgos *et al.* crayfish exoskeletons are used as raw material to evaluate the physicochemical and biological properties of the resulting CS. They conducted the following processes, demineralization with 4 mol L^{-1} HCl for 9 h, depigmentation with acetone for 18 h, deproteinization using 4 mol L^{-1} NaOH at 80 °C for 7 h and finally a deacetylation under drastic conditions NaOH 60 wt% at 120 °C for 9 h. The main characteristics of the CS were a moderate MW of 589.43 kDa and a DD of 91.55, which imparted enhanced solubility and improved capabilities for film and nanofiber formation with potential applications in biomedicine.[19] X-ray diffraction (XRD) and SEM analyses revealed CS has a lower crystallinity compared to its commercial counterpart; however, it demonstrated a denser and less porous structure. Its antioxidant capacity was evidenced by the inhibition of reactive oxygen species (ROS) at various concentrations (0–10 mg mL^{-1}), ranging from 0 to 44.57%, which surpassed the performance of commercial CS (0–29.58%). Furthermore, it exhibited significant antibacterial potential against *E. coli*, *S. typhimurium*, *L. monocytogenes* and *E. faecalis* with a minimum bactericidal concentration (MBC) lower than commercial CS.

The work of Rakshit *et al.* explored the conversion of CS from chitin, previously obtained from shrimp shell (*Litopenaeus vannamei*) by lactic acid treatment with the bacterium *Bacillus coagulans* L2 and the protease *Alcaligenes faecalis* S3. CS extraction was performed using the bacterium *Alcaligenes faecalis* C4, reaching an optimum enzymatic activity of 40.69 U mL^{-1}. The CS obtained presented outstanding characteristics, such as a DD of 74.9% and molecular weight (MW) of 246.4 kDa. FTIR and XRD analyses confirmed the presence of the α-chitosan structure with its characteristic functional groups and a low crystallinity index (21.16%) in enzymatically extracted CS (EEC) compared to chemically extracted chitosan (CEC), as shown in Fig. 2d. Previous studies performed with chitin from the same source reported similar values for DD (78%); however, a lower molecular mass (71.31 kDa) was obtained.[26] Regarding its biological properties, CS showed better antioxidant activity of 65.49% against 2,2-difenil-1-picrilhidrazilo (DPPH) radical at a concentration of 10 mg mL^{-1}. On the other hand, it presented antibacterial activity against *S. mutans*, *E. faecalis*, *E. coli* and *Vibrio* sp. whose minimum inhibitory concentration (MIC) values were 0.675, 1.75, 0.33 and 0.75 mg mL^{-1}, respectively.[3]

Wardhono *et al.* employed a reactor under constant ultrasonic irradiation with low frequency to evaluate the effects of time (<120 min) on the DD over a temperature range of 30 to 70 °C. They reported that the increase in DD is directly proportional to both the temperature and irradiation time, achieving 87.73%. FTIR analysis reveals a significant decrease in the intensity of the bands at 3260 and 3105 cm^{-1} in CS extracted *via* ultrasound, indicating that this extraction method directly affects the amine bonds (N–H) along the CS structure (Fig. 2e). The increase in the DD is further confirmed by the marked reduction of the band at 1660 cm^{-1}, associated with the carbonyl bond (C=O) of hydrolyzed acetamido groups.[28]

According to the study by Dong *et al.* microwave-assisted extraction of CS from the exoskeleton of white shrimp (*Penaeus vannamei*) directly influences its self-aggregation behavior in solution, conductivity, and solubility. Additionally, this method achieves a high DD (90.75%) as the number of microwave heating cycles increases. To evaluate its effect on CS properties, microwave heating at 250 W for 5 min was applied in multiple cycles throughout the deacetylation process. The extracted CS was characterized using FTIR spectroscopy, which revealed distinctive O–H and N–H bonds vibrations at 3263 cm^{-1}, 3421 cm^{-1}, and 3358 cm^{-1}, indicative of intermolecular interactions in polysaccharides. The degree of deacetylation was determined based on the absorbance of the amide III band, yielding values ranging from 84.9% to 90.75%. These findings confirm that microwave-assisted extraction significantly enhances the efficiency of the chitin deacetylation process. SEM analysis revealed a porous microfibril structure. However, an increase in the number of microwave heating cycles led to a substantial reduction in surface porosity, attributable to the reorganization of hydrogen bonds.[58] MW is a key parameter of CS that determinates its physicochemical and biological properties, as well as its potential applications.[47] In this work, MW was determined using the empirical Mark–Houwink–Sakurada equation. Increasing the number of microwave treatment cycles resulted in a significant decrease in MW of CS from 394.52 kDa to 67.88 kDa after four cycles. This effect is attributed to the molecular vibration induced by

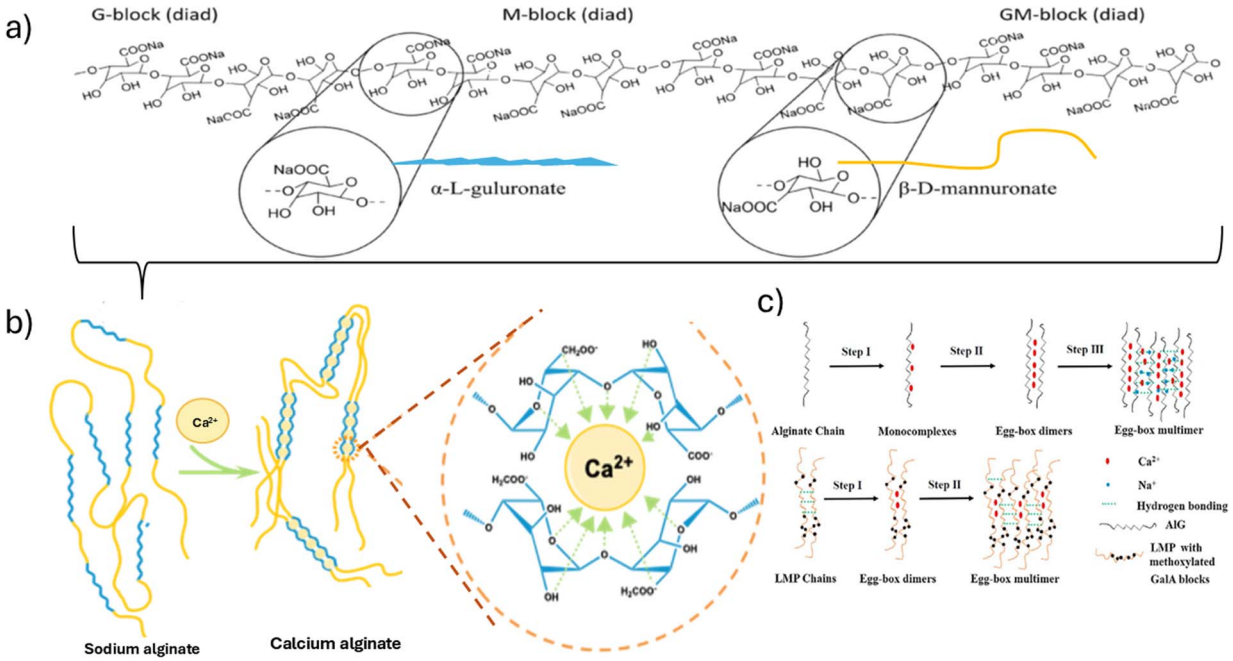

Fig. 3 (a) Molecular structure of sodium alginate, their components: α-L-guluronate (G) and β-D-mannuronate (M) and diad structures GG, MM and GM-blocks modified from ref. 2 copyright © 2021 published by Elsevier Ltd under the terms of Creative Commons CC-BY license. (b) Graphical description of the egg-box model for alginate gelation. Reproduced from ref. 60 copyright © 2023 The Authors. Published by Elsevier Ltd.; (c) illustrative scheme of possible junction points for alginate gelation and LMP, reproduced from ref. 61 copyright © 2020 Elsevier Ltd. All rights reserved.

microwave heating, which increases the contact area of chitin with the alkaline solution, favoring the hydrolysis of the β-1,4-glycosidic bonds. In addition, this decrease in MW was consistent with previous work involving microwave-assisted extraction of CS.[30]

3.2. Alginate

Alginate is a linear polysaccharide widely distributed in the cell walls of brown algae (*Phaeophyceae*) and certain bacteria, where it plays a crucial structural role by providing flexibility and mechanical strength. This anionic biopolymer consists of β-D-mannuronate (M) and α-L-guluronate (G) units, arranged in different proportions and sequences, which largely determine its physicochemical properties and industrial applications.[2] The structural composition of alginate can vary significantly depending on the algal species, environmental conditions, seasonality, and the extraction methods used[59] (Fig. 3a).

One of the most significant attributes of alginate is its ability to form gels in the presence of divalent cations, such as Ca^{2+}, through a cross-linking process that results in the egg-box structure.[62] In this model, divalent cations lodge into the cavities formed by two adjacent polymer chains containing GG blocks in helical conformations, enabling the formation of a stable three-dimensional network[60] (Fig. 3b).

The gelation capacity of alginate depends on numerous factors, including the proportion of M and G blocks, polymer chain length, and the type and concentration of the cross-linking agent. Generally, a high M/G ratio (>1) is associated with the formation of soft and elastic gels, while a low M/G ratio (<1) and a higher content of G blocks favor the formation of strong and rigid gels.[63] Additionally, alginate exhibits different affinities for various divalent cations in the following order: $Pb^{2+} > Cu^{2+} > Cd^{2+} > Ba^{2+} > Sr^{2+} > Ca^{2+} > Mg^{2+}$.[64] However, calcium is the most used cation due to its compatibility with biomedical and food applications.

Fig. 3c illustrates the steps of Ca-alginate-hydrogels formation through alginate and low methoxy pectin (LMP) cross-linking sites, which can be formed in the presence of G-rich blocks (GG) and, to a lesser extent, MG junctions. Due to its gel-forming ability and properties as a thickener, gelling agent, emulsifier, and stabilizer, alginate is widely used across various industries. In the food sector, it is employed as a texturizing agent and in the stabilization of emulsions. In the pharmaceutical and biomedical industries, alginate has established itself as a key polymer for drug encapsulation and controlled release of bioactive compounds.[59,65] Its biocompatibility and biodegradability have driven its application in tissue engineering and drug delivery systems. Moreover, its bioactive properties, including antioxidant, antimicrobial, and anti-inflammatory activities, have generated growing interest in health sciences and biotechnology.[7]

3.2.1. Conventional alginate extraction methods. Alginate extraction is a mass transfer process in which the solvent diffuses into the matrix, enabling the dissolution and isolation of bioactive compounds.[66] Extraction strategies include pre-treatments, cell disruption techniques, and both conventional and emerging methods, aiming to optimize the yield and quality of the biopolymer (Table 2 and Fig. 4a). The process

Table 2 Research studies are conducted to optimize alginate extraction conditions using different extraction methods

Sources	Extraction methods	Molecular weight (kDa)	M/G ratio	Key characteristics	Ref.
Laminaria ochroleuca	Chemical extraction	66–134	0.89–1.38	Moderate viscosity – molecular weight	63
Saccorhiza polyschides	Chemical extraction	53–73	1.62–2.14	Low molecular weight – viscosity	63
Halopteris scoparia	Chemical extraction	252	0.35	High molecular weight, significant anti-inflammatory and anticoagulant capacity	7
Cystoseira schiffneri	Chemical extraction	123–449	0.024–0.093	Antioxidant activity, high molecular weight	67
Cystoseira crinita	Chemical extraction	73.1	1.018	Low molecular weight, yield (20.18%), well-defined anti-inflammatory effects	65
Ascophyllum nodosum	Ultrasound assisted extraction	133–428	—	High viscosity – high molecular weight, high purity	2
Nizimuddinia zanardini	Ultrasound assisted extraction	360	—	High antioxidant and emulsifying capacity	68
Sargassum angustifolium	Enzyme extraction	357	0.54	High molecular weight – antioxidant property, good biological properties	65
Fucus vesiculosus	Enzyme assisted extraction	847	—	Higher molecular weight, low yield (9.60%), high purity (low content of protein and phenolic compounds)	69
Saccharina latissima	Ultra-high-pressure extraction	257.3	1.6	High molecular weight, high antioxidant capacity, good chelating agent	59
Saccharina latissimi	Microwave assisted extraction	419–458	—	High molecular weight, yield (20–24%), surface more smoothed and homogeneous	64

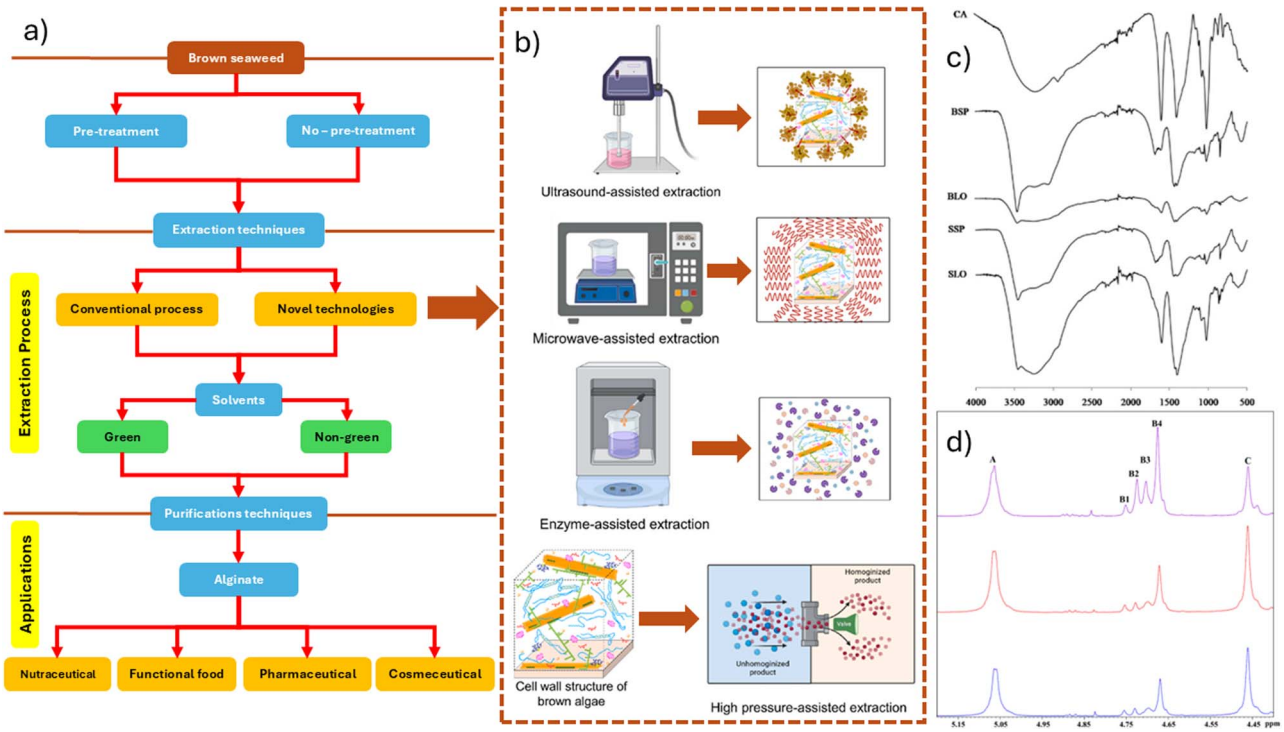

Fig. 4 (a) Overview of the alginate extraction processes and potential applications adapted from ref. 60 copyright © 2023 Elsevier Ltd. (b) Scheme of classification of extraction treatments assisted by novel technologies adapted from ref. 60 copyright © 2023 Elsevier Ltd. (c) FTIR spectra of commercial sodium alginate (CA) and alginates extracted from the blades *L. ochroleuca* (BLO), stipes of *L. ochroleuca* (SLO), blades of *S. polyschides* (BSP), and stipes of *S. polyschides* (SPS) adapted from ref. 63 copyright © 2022 under the terms and conditions of the CC BY license and (d) ^{1}H NMR spectra of purified alginate showing monads, diads and triads, purple represents food grade alginate, red represents unbleached extracted alginate, and blue represents bleached extracted alginate, reproduced with permission from ref. 66 copyright © 2020 Elsevier Ltd. All rights reserved.

typically begins with washing brown macroalgae with distilled water to remove salts, sand, and impurities. Two types of pre-treatments are then applied: the first facilitates cell wall disruption and enhances mass transfer, while the second prevents the co-extraction of bioactive compounds with similar solubility.[60] The conventional method for alginate extraction involves a pre-extraction step with mildly acidic solutions, followed by alkaline extraction, solid–liquid separation, precipitation, drying, and particle size reduction.[2] However, there is no standardized protocol, leading to multiple variations in industrial and scientific applications. These differences influence the molecular weight, mannuronic-to-guluronic acid ratio, and key technological properties such as purity, viscosity, and functionality.

One of the most widely used approaches is chemical extraction, which includes acid pre-treatment to remove unwanted compounds (*e.g.*, polyphenols and fucoidans), followed by alkaline extraction, where alginic acid is converted into sodium alginate. Precipitation and purification are then conducted using alcohol or calcium solutions, yielding alginate powder after drying and milling. This method produces alginates with moderate purity and viscosity, suitable for industrial applications in food, textile, and pharmaceutical sectors.[63,65]

3.2.2. Emerging alginate extraction methods. The increasing demand for more sustainable processes has driven the development of environmentally friendly extraction technologies (Fig. 4b). Innovative methods such as microwave-assisted extraction, ultrasound, high-pressure processing, pressurized fluid extraction, and enzyme-assisted extraction have been explored to improve process efficiency, reduce environmental impact, and enhance economic feasibility.[59,63] It is essential to note that extraction efficiency depends not only on process parameters but also on intrinsic factors such as the species and origin of the algae. This underscores the need to tailor extraction methods to specific biomass sources to optimize alginate recovery and quality.

Ultrasound-assisted extraction (UAE) is an emerging technique that utilizes ultrasonic waves to facilitate alginate release from cell walls, significantly reducing extraction time while preserving the structure of functional groups. This method yields alginates with higher molecular weight and viscosity, suitable for biomedical and cosmetic applications. Similarly, high-pressure processing (HPP) employs extreme pressure conditions to break algae cells and release alginate, enhancing process efficiency and producing alginates with high purity and molecular weight, ideal for industrial applications requiring improved rheological properties.[68]

Finally, enzymatic extraction of alginate is an efficient and sustainable alternative to conventional methods, as it enables the selective degradation of the macroalgal cell wall using specific enzymes, minimizing phenolic compounds and preserving the biopolymer's structure. Recent studies have optimized this process through technologies such as ultrasound and acid pretreatment, increasing yield and reducing extraction time.[62] Additionally, Bojorges, *et al.* highlighted how enzymatic treatments improve process efficiency and the quality of the extracted alginate. The combination of these approaches promotes a more sustainable extraction process and a product with enhanced properties for biomedical and biotechnological applications. The selection of the extraction method depends on the desired final application and the required properties, while advancements in these technologies promise to expand the applications of this versatile biopolymer in industries such as food, pharmaceuticals, and biomedicine.[60] The combination of these approaches promotes a more sustainable extraction process and a product with enhanced properties for biomedical and biotechnological applications. The selection of the extraction method depends on the desired final application and the required properties, while advancements in these technologies promise to expand the applications of this versatile biopolymer in industries such as food, pharmaceuticals, and biomedicine.

3.2.3. Characterization of alginate. The most common characterization techniques include FTIR and proton nuclear magnetic resonance (^{1}H NMR) analysis. The FTIR spectra of commercial alginate (CA) and sodium alginates extracted from *L. ochroleuca* (BLO) and *S. polyschides* (BSP) are presented in Fig. 4c. Despite differences in band intensity, all spectra exhibited a high degree of similarity. In the 3600–1600 cm^{-1} region, broad peaks centered at 3453 cm^{-1} and 3438 cm^{-1} were observed in all spectra, attributed to O–H stretching vibrations with hydrogen bonding. Weak signals at 3016 cm^{-1} in the blade spectra, and at 3033 cm^{-1} and 2937 cm^{-1} in the stipe spectra of BLO and BSP, respectively, were assigned to C–H stretching vibrations. Asymmetric stretching of carboxylate O–C–O vibrations was detected around 1600 cm^{-1} in all spectra, indicating a similar structure among the extracted alginates. The bands at 1404 cm^{-1} were attributed to C–OH deformation vibrations, with contributions from the symmetric O–C–O stretching of carboxylate groups.[63] These peaks are characteristic of sodium alginates with an M/G ratio greater than 1, indicating a high content of mannuronic acid units. The composition of alginate in terms of its guluronic and mannuronic acid residues (G and M blocks) is a key property that significantly influences its gelling capacity. ^{1}H NMR spectroscopy is the primary technique used to investigate the sequence of these uronic acids. Fig. 4d shows the anomeric protons and other protons at different carbon positions within the uronic acid sequence. The chemical shifts of the characteristic protons of the alginate extracted from *S. natans* (bleached and unbleached) and the commercial food-grade alginate exhibit a strong correlation, confirming the nature of the extracted product. The block structure and M/G ratio were determined following the ASTM F2259-10 standard.[66] Gel permeation chromatography (GPC) evaluates molecular weight, influencing viscosity and the ability of alginate to form films, while thermal analysis *via* Thermogravimetric Analysis (TGA) and Differential Scanning Calorimetry (DSC) examines thermal stability and degradation properties, critical for biomedical and food applications.[2]

Ultrasound-assisted extraction from *Ascophyllum nodosum* produces alginate with a molecular weight between 133–428 kDa and high viscosity, making it suitable for applications requiring high strength, such as the food sector and cell encapsulation.[2] Similarly, alginate extracted from *Nizimuddinia*

zanardini exhibits a molecular weight of 360 kDa and is notable for its antioxidant and emulsifying capacities, valuable for cosmetic and food formulations.[68] For *Laminaria ochroleuca*, chemical extraction yields alginate with a molecular weight between 66–134 kDa and a moderate M/G ratio (0.89–1.38), offering moderate viscosity ideal for gelling applications with good handling properties.[63] Meanwhile, *Halopteris scoparia* produces alginate with a high molecular weight of 252 kDa, featuring anti-inflammatory and anticoagulant properties, making it an ideal candidate for tissue engineering and therapeutic applications.[7,67]

Ultra-high-pressure and microwave extraction from *Saccharina latissima* produces alginates with molecular weights between 419–458 kDa and high surface homogeneity, making them suitable for controlled-release and cell support applications.[59] On the other hand, enzymatically extracted alginate from *Fucus vesiculosus* exhibits a molecular weight of 847 kDa, with high purity and low protein and phenolic compound content, characteristics ideal for medical devices and cosmetics.[69] Finally, alginates from *Cystoseira schiffneri* and *Cystoseira barbata* have molecular weights ranging from 123–449 kDa and a low M/G ratio, contributing to their high antioxidant activity and emulsifying capacity, valuable in the food industry.[65,67] Each extraction method and algal species significantly influence the final properties of alginate, determining its applicability in various industrial fields. High molecular weight and purity alginates excel in biomedical and food applications requiring specific properties like high viscosity, antioxidant capacity, or biocompatibility, while lower molecular weight alginates are suited for formulating flexible materials and controlled release systems.

3.3. Pectin

Pectin is a polysaccharide-based carbohydrate polymer found in the primary cell walls and middle lamella of plants, primarily composed of galacturonic acid (Gal-A) in three structural forms: rhamnogalacturonan I, rhamnogalacturonan II, and homogalacturonan. Depending on the degree of esterification (DE), pectin is classified as low methoxyl pectin (DE < 50%) and high methoxyl pectin (DE > 50%), as illustrated in Fig. 5a. Low methoxyl pectin gelation, explained by the "egg-box model," requires calcium ions (Ca^{2+}), while high methoxyl pectin forms gels under acidic conditions and with high sugar content. Electrostatic interactions, hydrogen bonds, and van der Waals forces stabilize low methoxyl pectin gels, whereas high methoxyl pectin involves esterification of carboxylic groups, reducing hydrophilicity and hydrogen bonding.[70] Owing to its tunable structure and to processing-dependent properties such as molecular weight, degree of esterification, and rheology-pectin is a workhorse polysaccharide used across the food sector (gelling, stabilizing, thickening) and biomedicine (drug delivery, wound healing, tissue engineering); extraction and purification ultimately determine application fit.[71] Consequently, pectin remains central to biopolymer technology and an active focus within carbohydrate polymer research.[72] By modifying the chemical structure of pectin, researchers have enhanced its mechanical strength, water retention capacity, and functional interactions with bioactive compounds. The increasing demand for eco-friendly materials has also driven the development of pectin-based hydrogels, films, and nanocomposites, reinforcing their role as a multifunctional polysaccharide.

3.3.1. Methods of pectin extraction. Advancements in extraction methods have transitioned from using ethanol or inorganic acid aqueous solutions to more eco-friendly solvents like hot water and citric acid.[75] Novel techniques, such as ultrasound-assisted, microwave-assisted, enzymatic, subcritical water, and pulsed electric field extractions (Fig. 5a), have emerged.[75,76] These unconventional methods reduce extraction time and temperature while achieving competitive efficiency tailored to various applications.[70] For instance, ultrasound extraction yields pectin with moderate molecular weight and high active functional group content, ideal for thermal stability and antioxidant activity. Enzymatic extraction produces pectin with lower phenolic compound content and excellent emulsifying properties, suitable for food and biomedical applications. Subcritical water extraction creates homogeneous pectin with outstanding stability, optimal for encapsulation and controlled release. Microwave-assisted extraction has demonstrated yields of up to 21.5% in minimal time, enhancing pectin's physicochemical properties by altering cell structure and improving solvent penetration.[8,70,76,77]

3.3.2. Characterization of pectin. Fig. 5b highlights the FTIR analysis to determine pectin's suitability for specific applications. This spectrum identifies key functional groups such as –OH, –COO, and –C=O, which influence gelation properties. ^{1}H NMR evaluates pectin's chemical structure, Fig. 5c, particularly galacturonic acid content and esterification degree, directly impacting gel-forming ability and behavior under varying pH conditions. Fig. 5d shows the HPLC analysis, which provides molecular weight distribution data and chemical composition, influencing viscosity and film-forming capacity. Thermal analyses, such as TGA and DSC, assess thermal stability and degradation properties, essential for applications involving high temperatures and pharmaceutical use.[75,78]

The unique properties of pectin vary significantly depending on its source and extraction method, as shown in Table 3. Subcritical water extraction from *Flos magnoliae* yields pectin with a molecular weight of 99.20–278.69 kDa and high galacturonic acid content, conferring excellent antioxidant activity suitable for food and pharmaceutical applications requiring antioxidant protection.[4] Ultrasound extraction from *Citrus limetta* peels produces pectin with a high molecular weight (541.61 kDa) and moderate esterification degree, imparting superior thermal and antioxidant properties, which are essential for cosmetic and food formulations where stability is critical. As depicted in Fig. 5e, the pectic extracted by UAE exhibits shaper peaks compared to commercial pectin; however, both display similar crystalline and amorphous portions.[74] Enzymatic extraction from sugar beet pulp generates pectin with a lower molecular weight (115–132 kDa) and good emulsifying capacity, making it ideal for controlled interactions in food and

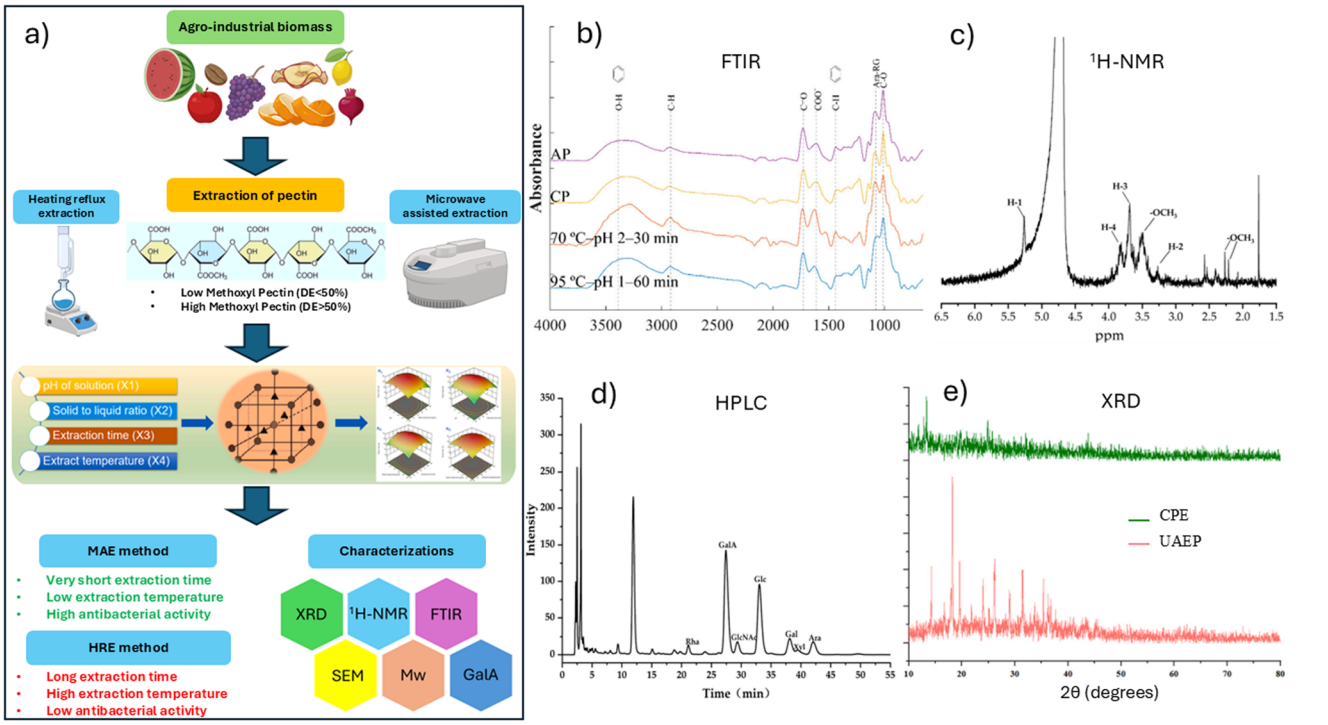

Fig. 5 (a) A comparative diagram of extraction of pectin from agro-industrial biomass using conventional heating reflux extraction (HRE) and microwave assisted extraction (MAE) techniques, optimization procedure and characterization, reproduced from ref. 70 copyright © 2023 Elsevier Ltd. All rights reserved. (b) FTIR spectra of watermelon rind pectin (WRP) extracted at mild and harsh conditions in comparison with commercial apple pectin (AP) and citrus, reproduced from ref. 73 copyright © 2021. License MDPI, under the terms and conditions of the (CC BY). (c) ^{1}H NMR spectrum of pectin extracted from coffee husk; (d) composition of Arabica coffee husk determined by high-performance liquid chromatography (HPLC) reproduced from ref. 8 copyright © 2023. License MDPI, under the terms and conditions of the CC BY license. (e) XRD patterns of commercial pectin (CP) and ultrasound extracted citrus pectin (UAEP). Reproduce from ref. 74 copyright © 2022 Elsevier Ltd. All rights reserved.

pharmaceutical products requiring sustained release.[79] Chemical extraction from watermelon rind results in pectin with a low molecular weight (106.1 kDa) and a highly branched structure, enhancing protein interaction for edible films and biomaterial production.[73] Ultrasound extraction from pineapple peels provides pectin with high thermal stability and excellent gel-forming properties, advantageous for applications that require firm gels at varying temperatures, such as in food and tissue engineering products.[75] Subcritical water extraction from apple residues yields pectin with a wide molecular weight range (9.8–697.6 kDa) and adjustable antioxidant capacity, suitable for bioactive compound encapsulation and pharmaceutical matrices.[76] Lastly, enzymatic extraction from coffee husks produces pectin with an extremely high molecular weight (1040 kDa) and a compact structure, making it ideal for applications involving controlled release and high solution stability.[78] The extraction method and source of pectin significantly influence its properties, such as molecular weight, esterification degree, and compound interaction capacity, directly affecting its applicability. High molecular weight and homogeneous structure pectin excel in food and pharmaceutical applications requiring stable gels and antioxidant capacity. In contrast, low molecular weight pectin is more effective for controlled-release applications. Optimizing synthesis and characterization methods enables the development of materials tailored to specific industrial demands.

3.4. Cellulose

Cellulose is a polysaccharide-based carbohydrate polymer and the most abundant biopolymer in nature. It consists of linear chains of repeating β-D-glucose units linked by β-(1 → 4)-glycosidic bonds, forming the primary structural component of plant cell walls.[1] As a well-characterized carbohydrate polymer, cellulose plays a crucial role in structural support, water retention, and mechanical properties in biological systems. In addition to plant-derived sources, cellulose can be obtained from bacterial sources such as *Acetobacter xylinum*, which produces cellulose with high purity, crystallinity, and excellent water retention capacity. This bacterial cellulose is particularly valuable for biomedical, tissue engineering, and pharmaceutical applications due to its superior physicochemical properties.[81]

Given its carbohydrate polymer nature, cellulose has unique physicochemical characteristics that make it essential in diverse industrial applications. Its high crystallinity, biodegradability, and chemical reactivity enables its use in food packaging, pharmaceuticals, textiles, and biomaterials.[82] The extraction and modification of cellulose significantly impact on

Table 3 Pectin characteristics according to its source and extraction method

Source	Extraction methods	Molecular weight (kDa)	Functional groups	Gal-A content (%)	Key characteristics	Ref.
Watermelon rind	Chemical extraction	106.1	–OH, –CH, –C=O, –COO, –NH	54.03	Lower molecular weight, higher protein interaction, higher degree of branching	73
Citrus fruit (*Citrus sinensis*)	Chemical extraction	200.6	–OH, –CH, –COOH, –COO, COC	50.56	Higher molecular weight and viscosity, generates strong gels with a stable structure	72
Dragon fruit peel	Chemical extraction	1181.76	–OH, –CH, –C=O, –COO	87.02	Excellent emulsifying and antioxidant properties, smooth surface with slight creases	80
Finger citron pomace	Ultrasound assisted extraction	127.5–218.1	–OH, –CH, –C=O	75.04–80.91	High viscosity, rounded and granular surface, excellent stability in solution	77
Citrus limetta peel	Ultrasound assisted extraction	541.61	–OH, –CH, –C=O, –COC, –COO	79.60	Moderate degree of esterification (59.71%), compact structure and smooth surface, better thermal and antioxidant properties	74
Pineapple peel	Ultrasound assisted extraction	182	–OH, –CH, –COO, –C=O, –C–O		High thermal stability, high crystallinity, good gelling properties	75
Coffee husks	Enzyme assisted extraction	1040	–OH, –CH, –C=O, COC	45.01	High molecular weight, good antioxidant properties, compact and rough structure	78
Sugar beet pulp	Enzyme assisted extraction	115–132	–OH, –CH, –C=O, –COO, –CN	48.91–57.13	Moderate emulsifying property, low degree of esterification	79
Flos magnoliae	Subcritical water extraction	99.20–278.69	–OH, –C=O, –CH, –COO, –COC	—	Particles are largely irregular and flaky with some small pores, exhibit stronger antioxidant activity	4
Apple pomace	Subcritical water extraction	9.8–697.6	–OH, –CH, –NH, –C=O, –COO	12.63–68.62	High weight: good gelling properties, low weight: high antioxidant activity	76
Jackfruit rags (*Artocarpus heterophyllus*)	Microwave assisted extraction	232.75	–OH, –CH, –C=O, –COO, –COC	61.53	Non-compact surface with some irregularities, higher viscosity, high antimicrobial activity	70
Grape pomace (*Feteasc̆ă neagr̆ă*)	Microwave assisted extraction	45.4	–OH, –CH, –C=O, –COO, –C=C, –C–O	81.24	Rough and brittle structure, good emulsifying capacity, low molecular weight	71

its molecular structure, crystallinity index, and mechanical strength, which determine its suitability for various functional applications.[83] To fully leverage cellulose as a functional carbohydrate polymer, understanding its extraction methods and characterization techniques is crucial. The following sections discuss the most relevant techniques to obtain high-purity polysaccharide-based cellulose and how its properties are analyzed for advanced material applications.

3.4.1. Methods of cellulose extraction. The extraction and synthesis methods directly influence the final structure and functionality of cellulose, affecting its degree of polymerization, crystallinity, and molecular weight. The recovery of high-purity cellulose requires the efficient removal of hemicellulose, lignin, and other non-cellulosic materials, with each method presenting specific advantages and limitations (Fig. 6a).

3.4.2. Conventional extraction methods for cellulose. Some conventional extraction methods such as acid hydrolysis achieve high crystallinity but may lead to cellulose degradation. Acid hydrolysis facilitates the decomposition of hemicellulose and cellulose in the presence of acidic catalysts such as HCl, HNO_3, and H_2SO_4, enabling efficient isolation.[87] The efficiency of this process is highly dependent on acid concentration, reaction temperature, and duration, as prolonged hydrolysis can lead to complete cellulose breakdown, disrupting its crystallinity.[88] Typically, wheat straw undergoes reflux in acetic acid, followed by bleaching with $NaClO_2$ and a NaOH buffer at 70 °C. Subsequently, the extracted cellulose is subjected to hydrolysis using strong acids for 24 h, enhancing its purity and crystallinity.[89] Despite its efficiency in cellulose recovery, this method poses challenges such as equipment corrosion and high purification costs.[90]

As an alternative, solid acids have been proposed to reduce corrosivity and operational risks.[89] Another conventional extraction method is alkaline treatment using NaOH enables the selective solubilization of lignin, thereby facilitating cellulose extraction in a shorter time and with reduced chemical harshness.[91] The application of 17.5% NaOH for 2 h at 25 °C has been demonstrated to effectively remove soluble components, including lignin.[92] Subsequently, the cellulose is bleached with H_2O_2. Following acid hydrolysis, a second alkaline treatment with 2% NaOH at 80 °C for 2 h is performed, followed by an additional $NaClO_2$ bleaching step.[93] This method effectively removes residual phenolic compounds and proteins, yielding cellulose with a purity of 84.67%.[84] Alkaline hydrolysis allows for efficient extraction with minimal structural damage, offering a more sustainable approach.

3.4.3. Eco-friendly and advanced extraction methods. Meanwhile, solvent-based extraction is emerging as a promising alternative for obtaining high-purity cellulose with reduced environmental impact. The use of solvents facilitates the efficient hydrolysis of hemicellulose and lignin, yielding cellulose with high purity and recovery rates. Combinations of polyethylene glycol (PEG) with salts and aqueous HCl have been shown to be effective, achieving cellulose recovery rates between 48.9% and 55.5%, with minimal hemicellulose (1.2–3.2%) and lignin (0.97–3.47%) content.[94] This method enhances the dissolution of non-cellulosic components and enables the regeneration of cellulose in a highly crystalline and pure.[95] Although considered a cleaner alternative to acid hydrolysis, some solvents may require post-treatment removal to prevent residual contamination.[84]

Innovative methods for cellulose extraction emerged due to the limitations of conventional cellulose extraction techniques. These alternative approaches are designed to enhance efficiency and sustainability while minimizing equipment degradation and purification costs (see Fig. 6a). One such approach is microwave-assisted extraction, which utilizes microwave energy to heat solvents uniformly, enhancing thermal efficiency and reducing reaction times.[96] A study demonstrated that subjecting wheat straw to acid pretreatment at 80 °C, followed by microwave digestion with NaOH (1–5%) at 100 °C for 20 min, led to a 67% reduction in reaction time, yielding cellulose with 90.66% purity and a crystallinity index of 42.50–60.56%.[88] Additionally, fractionation and mechanical fibrillation have been employed to produce lignocellulosic nanofibrils (LCNFs) with reduced lignin and ash content, making them suitable for biodegradable composites and packaging materials.[97]

Another promising technique is organosolv fractionation, which efficiently separates cellulose, hemicellulose, and lignin using organic solvents such as 1,4-dioxane, methanol, ethanol, and acetone.[87] This method offers high selectivity in isolating cellulose while maintaining its structural integrity. Moreover, steam explosion and microfluidization have been explored as energy-efficient alternatives, requiring 70% less energy than traditional milling methods, while simultaneously enhancing cellulose crystallinity and purity.[98] The TEMPO (2,2,6,6-tetramethylpiperidin-1-yl)oxyl oxidation process, an advanced chemical modification technique, introduces carboxyl (–COOH) groups to the cellulose surface, thereby improving water dispersibility and mechanical stability, making it highly suitable for nanocellulose applications. Furthermore, enzymatic hydrolysis has emerged as a biological and eco-friendly approach, wherein specific cellulolytic enzymes selectively degrade amorphous cellulose, yielding cellulose nanocrystals (CNCs) with high crystallinity.[84] This enzymatic process also allows for biomass recycling, making it a sustainable alternative for cellulose extraction. Collectively, these novel methodologies represent a significant advancement over conventional processes, optimizing cellulose yield, purity, and crystallinity while reducing chemical usage and environmental impact.

The chemical structure of cellulose, hemicellulose, and lignin is illustrated in Fig. 6b. The intricate multilevel architecture of cellulose consists of bundles or aggregates of ultrafine fibrils, where multiple cellulose chains are embedded within the superfine fibril structure. Table 4 highlights how cellulose properties vary based on source and extraction method, directly influencing its industrial applications. Plant-derived cellulose (crystallinity 40–70%) is widely used in paper and textiles, while bacterial cellulose (crystallinity >80%) is preferred in biomedicine due to its strong, porous films ideal for wound dressings and tissue regeneration.[1] Nanocellulose, produced through high-energy methods, offers high aspect ratio and mechanical strength, making it suitable for composites and functional coatings.[81]

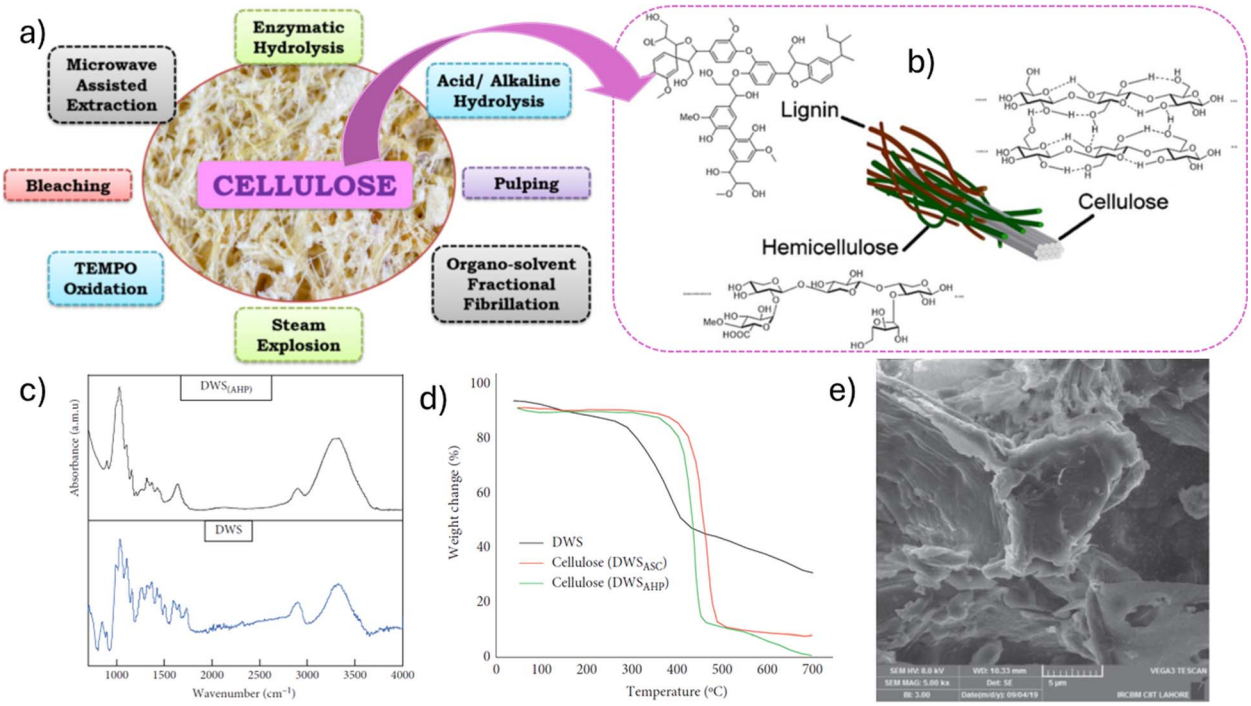

Fig. 6 (a) Different cellulose extraction methods reproduced from ref. 84 copyright © 2022 Elsevier B.V. All rights reserved. (b) Chemical structure of cellulose, hemicellulose, and lignin reproduced from ref. 85 copyright © 2023. Published by Elsevier Ltd under the terms of the CC-BY license. (c) FTIR characterization of isolation of cellulose through Alkaline Hydrogen Peroxide (AHP) Treatment and DWS; (d) thermogravimetric analysis of DWS and cellulose with AHP and ASC treatment; (e) SEM image of cellulose after $DWS_{(AHP)}$ reproduced from ref. 86 copyright © 2020 under the Creative Commons Attribution License.

Enzymatically hydrolyzed cellulose (100–250 kDa) enhances dispersion and thermal stability, making it ideal for pharmaceuticals and food formulations requiring controlled release. Ultrasound and enzymatic hydrolysis improve both extraction efficiency and cellulose properties, optimizing performance for specific applications.[84] Crystallinity dictates cellulose functionality: high-crystallinity cellulose provides mechanical strength and thermal stability, ideal for advanced engineering, while low-crystallinity cellulose is suited for flexible, absorbent products like diapers and hygiene items. Additionally, nanocellulose shows high potential in electronics, enabling flexible devices and high-performance batteries. Selecting the appropriate extraction and characterization methods is crucial to optimizing cellulose properties for targeted industrial applications.[8,100]

For characterization, American Society for Testing Materials (ASTM) standards were employed to determine the chemical composition of treated and untreated fibers. The quantification of α-cellulose, lignin, and holocellulose was performed following ASTM D1103-55T, ASTM D1106-56, and ASTM D1104-56, respectively.[86] FTIR analysis (Fig. 6c) was conducted to assess the presence of cellulose, hemicellulose, and lignin before and after treatment. The extracted cellulose exhibited characteristic absorption bands, where peaks at 1644 cm^{-1} and 895 cm^{-1} corresponded to –OH bending of absorbed water and asymmetric ring stretching of cellulose, respectively. The disappearance of bands at 1735 cm^{-1} and 1248 cm^{-1} confirmed the removal of lignin and hemicellulose, consistent with previous studies.[86,103] XRD analysis revealed that the peak at 22.5° indicated the presence of type I cellulose polymorph, suggesting that the treatment did not alter cellulose polymorphism. An increase in crystallinity was observed, attributed to the efficient removal of non-cellulosic components.[104] As shown in Fig. 6d, TGA was used to evaluate the thermal stability of the extracted cellulose. Due to the chemical differences between cellulose, hemicellulose, and lignin, their degradation occurred at distinct temperatures.[103]

For dewaxed wheat straw (DWS), thermal degradation occurred in three stages: onset at 180 °C (hemicellulose and cellulose degradation), second stage at 254 °C (overlapping degradation of cellulose and lignin), and maximum degradation peak at 304 °C. For cellulose isolated *via* Acidified Sodium Chlorite (ASC) treatment (DWS_{ASC}), degradation began at 310 °C, with a decomposition temperature of 385 °C. In contrast, for cellulose extracted through Alkaline Hydrogen Peroxide (AHP) treatment (DWS_{AHP}), degradation started at 304 °C and completed at 360 °C. The enhanced thermal stability of treated fibers was attributed to the removal of lignin and hemicellulose, which improved the structural organization of the material.[103] SEM micrographs (Fig. 6e) confirmed morphological differences in the extracted cellulose, highlighting the impact of chemical treatments on wheat straw fibers. The reduction in fiber volume and diameter observed in SEM images was consistent with previous studies.[103] The physical appearance of DWS changed after the AHP treatment, the extracted fibers acquired a pure white color, indicating the effective removal of

Table 4 Characteristics of cellulose based on precursor and extraction method

Biopolymer	Sources	Extraction methods	Yield (%)	Functional groups	Key characteristic	Ref.
Nano cellulose	Sugarcane bagasse	Chemical extraction	65	–OH, –CH, –C═O	High thermal stability and crystallinity, great antibacterial properties (*Bacillus* and *E. coli*)	1
Nano cellulose	Date palm fiber (*Phoenix dactylifera*)	Chemical extraction	57.1	–OH, –CH, –COC	High nanometer surface area, rod-like shape and high thermal resistance	81
Cellulose	Pine cones	Chemical extraction	37.38	–OH, –CH, –COO, –COC, –C–C	Low crystallinity index (39.59%), surface apparently rough and irregular, maximum degradation temperature (339 °C)	99
Cellulose	Three (*Alstonia scholaris*)	Chemical extraction	68	–OH, –CH, –C═O, –COH, –C═C	High Young's modulus and flexibility, crystallinity (68%), improved thermal stability	83
Nano cellulose	Areca nut husk	Chemical extraction	32	–CO, –CH, –OH	High crystallinity index (90%) and thermal stability, individual needle shaped structures	87
Cellulose	Agro-waste seeds (*Tamarindus indica*)	Chemical extraction	90.57	–OH, –CH, –C═C, –C═O, –COO	High yield and crystallinity index (77.6%), rough surface with small apertures, good thermal stability	100
Cellulose	Agricultural waste (*Camellia oleifera*)	Chemical extraction	42.13	–OH, –CH, –C–O	Increased thermal stability and encapsulation efficiency, loaded with essential oil present higher antibacterial activity against *S. aureus* and *E. coli*	8
Cellulose	Rice straw waste	Ultrasound assisted extraction	53.02	–OH, –COC, –CH	Good crystallinity index (64.50%), rough and irregular fiber surface	88
Cellulose	Rice straw	Ultrasound assisted extraction	28.2	–OH, –C═O, –CH, –COO, –COC	Cellulose films: tensile strength (4.06–5.22 MPa), Young's modulus (101.05–200.83 MPa), high purity (93.37%), nanocellulose: high crystallinity (88.66%)	101
Cellulose	Date palm trunk (*Phoenix dactylifera*)	Supercritical fluid extraction	66.53	–OH, –CH, –COC	Good thermal stability, good crystallinity (68.60%), fibers with smooth surface	102

lignin and hemicellulose. The physical appearance of DWS changed after the AHP treatment, the extracted fibers acquired a pure white color, indicating the effective removal of lignin and hemicellulose.[86]

4. Antimicrobial activity of the biopolymers

The antimicrobial activity of biopolymers can be enhanced through chemical modification and the incorporation of bioactive agents, such as essential oils or organic extracts.[105] These systems have demonstrated efficacy against both Gram-positive and Gram-negative bacteria due to their ability to interact with microbial membranes, resulting in cell wall disruption and lysis.[106] Table 5 summarizes the potential of biopolymer-based materials to inhibit the growth of many different bacteria.

4.1. Cellulose-based nanocomposites

The antimicrobial efficacy of cellulose is improved when employed as a carrier matrix for essential oils, particularly in its nanostructured form such as nanocellulose and nanofibers.[119] Abral *et al.* developed bacterial nanocellulose (BNC) *via Acetobacter xylinum* fermentation followed by mechanical homogenization and ultrasonication. The resulting nanofibers were incorporated into a composite matrix composed of chitosan and tapioca starch to fabricate biofilms with varying BNC loadings of 10, 15, and 20 mL. Mechanical performance improved significantly, particularly in elongation at break, which reached 43.7, 20.9, and 21.0%, respectively. Antimicrobial activity was evaluated against *Staphylococcus aureus*, *Bacillus subtilis*, *Escherichia coli*, and *Pseudomonas aeruginosa*. Films containing 20 mL BNC exhibited the highest inhibition zones 14.5, 10.6, 10.3, and 13.4 mm, respectively. These effects are attributed to the synergistic mechanisms between the nanocellulose structure, which increases surface reactivity, and the chitosan matrix, known for its intrinsic antimicrobial properties.[120] Among the various essential oils explored for their antimicrobial efficacy, cinnamon essential oil (CEO) has attracted significant attention due to its chemical bioactive constituent, cinnamaldehyde, which interferes with critical cellular processes.[121] This feature enables CEO to act more effectively against pathogens with complex membrane structures, as demonstrated by Stasiak-Różańska *et al.* In their study, bacterial cellulose (BC) was impregnated with a range of essential oils, and CEO-loaded BC composites exhibited the highest antimicrobial activity against multiple *Cronobacter* species. Notably, inhibition zone diameters of 34.62 mm for *Cronobacter muytjensii*, 29.05 mm for *Cronobacter condimenti*, and 32.10 mm for *Cronobacter malonaticus* were recorded, confirming the potent antibacterial nature of cinnamon–cellulose nanocomposites.[107]

4.2. Chitosan-based nanocomposite

The intrinsic antimicrobial activity of chitosan can be significantly enhanced through the incorporation of functional bioactive agents.[122] For instance, chitosan films enriched with *Cinnamodendron dinisii* essential oil encapsulated in zein exhibited a remarkable ability to extend the shelf life of ground beef by reducing spoilage reactions during refrigerated storage.[110] Similarly, chitosan and polyvinyl alcohol (PVA) films containing essential ginger oil effectively inhibited the growth of *S. aureus*, *E. coli*, and *P. fluorescens*, thereby prolonging the preservation of sea bass fillets.[112] Fig. 7a–d illustrates the antibacterial activity assessment (A and B) and inhibition zone measurement (C and D) of films based on pectin, pectin/CH, and CH, incorporated with noni fruit extract at varying concentrations. These films were evaluated against Gram-negative bacteria (*E. coli* and *S. typhimurium*) and Gram-positive bacteria (*S. aureus* and *L. monocytogenes*). Lowercase letters (a–g) indicate statistically significant differences ($p < 0.05$) in the inhibition zone among different film types against the tested bacteria, while uppercase letters (A, B) denote significant differences ($p < 0.05$) in the inhibition zone of the same films when tested against different bacterial strains. Negative control (NC) consisted of distilled water, while positive control (PC) used tetracyclines at 5 mg mL^{-1}.[116]

4.3. Alginate-based nanocomposites

Although alginate inherently lacks pronounced antimicrobial properties, its bioactivity can be significantly enhanced through the incorporation of bioactive agents. Fig. 7e presents the inhibition zone (ZOI) assessment of the prepared SA/Cur and SA/Cur–PLA hydrogel beads against Gram-negative (*E. coli*, *P. aeruginosa*) and Gram-positive (*S. aureus*, *S. pyogenes*) bacteria at different concentrations (5–250 μg mL^{-1}), ampicillin as a standard used as positive control; no statistical comparison was performed. The results showed that SA/Cur–PLA beads exhibited higher antibacterial activity at higher concentrations (250 μg mL^{-1}), whereas no effect was observed at lower concentrations (5 μg mL^{-1}), possibly due to limited curcumin availability. ZOI increased with bead concentration, reaching values comparable to those of standard ampicillin, suggesting that both SA/Cur and SA/Cur–PLA possess antimicrobial properties.[116] Recent studies have demonstrated that the integration of antimicrobial microcrystalline cellulose (AMCC) and probiotic strains into edible alginate films improves their effectiveness against pathogens, while also providing mechanical stability and reducing water vapor permeability.[109] These films have proven particularly effective in preserving ultrafiltered (UF) cheeses, ensuring the viability of probiotic bacteria for more than 45 days. On the other hand, bacterial cellulose, despite lacking intrinsic antimicrobial activity, has been used as a reinforcement in biopolymer matrices. When combined with ginger essential oil, bacterial cellulose nanofibers have enhanced the antimicrobial properties of chitosan/PVA-based films, demonstrating efficacy against *E. coli* and *S. aureus* in fish packaging.[112]

4.4. Pectin-based nanocomposites

Pectin is a biopolymer capable of forming biodegradable films, but its antimicrobial activity is relatively low compared to other polymers. Nevertheless, its combination with essential oils and

Table 5 Antimicrobial activity of different biopolymers against Gram-positive and Gram-negative bacteria

Biopolymers	Modifications	Microorganisms	Diameter of inhibition zone (mm)	Key characteristics	Ref.
Cellulose nanofiber	Starch/chitosan	*Staphylococcus aureus*	14.5 ± 5.8	Environmentally friendly edible biocomposite	107
		Bacillus subtilis	10.6 ± 4.9		
		Escherichia coli	10.3 ± 1.5		
		Pseudomonas aeruginosa	13.4 ± 3.3		
Nanocellulose sponge	Propolis extract	*Staphylococcus aureus*	3.0 ± 0.1	Effective impregnation and retention of propolis on the nanocellulose surface	105
		Pseudomonas aeruginosa	3.0 ± 0.3		
Bacterial cellulose	Cinnamon essential oil	*Cronobacter muytjensii*	34.62 ± 1.51	High loading capacity and sustained retention of essential oils	108
		Cronobacter condimenti	29.05 ± 1.78		
		Cronobacter malonaticus	32.10 ± 0.87		
Chitosan film	Microcrystalline cellulose	*Staphylococcus aureus*	20.0 ± 0.50	Good mechanical properties, probiotic edible film	109
		Listeria monocytogenes	14.0 ± 0.33		
		Aspergillus niger	15 ± 0.33		
Chitosan	*Cinnamodendron dinisii* essential oil	*Staphylococcus aureus*	5.0–8.0	Good antioxidant and antimicrobial activity	110
		Escherichia coli	5.0–8.0		
		Salmonella typhimurium	8.0–12.0		
		Shigella flexneri	8.0–12.0		
Chitosan nanofiber	Gelatin/curcumin	*Staphylococcus aureus*	17.25 ± 0.12	Improved antioxidant activity and sensitivity to ammonia	111
		Escherichia coli	16.07 ± 0.29		
Chitosan film	Polyvinyl alcohol/*Lateolabrax japonicus* essential oil	*Staphylococcus aureus*	15.65 ± 0.38	Great tensile strength and barrier performance	112
		Escherichia coli	14.92 ± 0.05		
		Pseudomonas fluorescens	13.62 ± 0.11		
Alginate	Curcumin/polylactic acid	*Escherichia coli*	18.0	Improvement in viscosity and solubility	113
		Pseudomonas aeruginosa	17.0		
		Staphylococcus aureus	17.0		
		Streptococcus pyogenes	16.0		
Alginate film	Carboxymethyl cellulose/*Thymus vulgaris* extract	*Staphylococcus aureus*	9.17	Enhanced antioxidant activity and water contact angle	114
		Escherichia coli	11.87		
		Bacillus cereus	14.12		
		Salmonella typhimurium	10.71		
Alginate	Gelatin/*Pimpinella anisum* essential oil	*Escherichia coli*	19.3 ± 0.52	Improved elongation at break, water permeability and contact angle	115
		Staphylococcus aureus	24.61 ± 0.66		
		Saccharomyces cerevisiae	22.33 ± 0.83		
		Aspergillus niger	23.16 ± 0.74		
Alginate	Microcrystalline cellulose	*Staphylococcus aureus*	25.0 ± 0.88	Good mechanical properties, probiotic edible film	109
		Listeria monocytogenes	20.0 ± 0.30		
		Aspergillus niger	18 ± 0.33		
Pectin film	Chitosan/*Morinda citrifolia* extract	*Escherichia coli*	9.21–11.00	Increased tensile properties and water vapor permeability	116
		Salmonella typhimurium	8.68–10.56		
		Staphylococcus aureus	8.47–11.42		
		Listeria monocytogenes	9.30–12.64		
Pectin	*Morus alba* leaf extract	*Pseudomonas aeruginosa*	15.78 ± 0.06	Great biocompatibility and improved mechanical properties	117
		Bacillus cereus	18.08 ± 0.01		
Pectin	Chayote tuber starch/cinnamon essential oil	*Staphylococcus aureus*	20–40	Excellent sustained-release and beef preservation properties	118
		Escherichia coli	20–40		

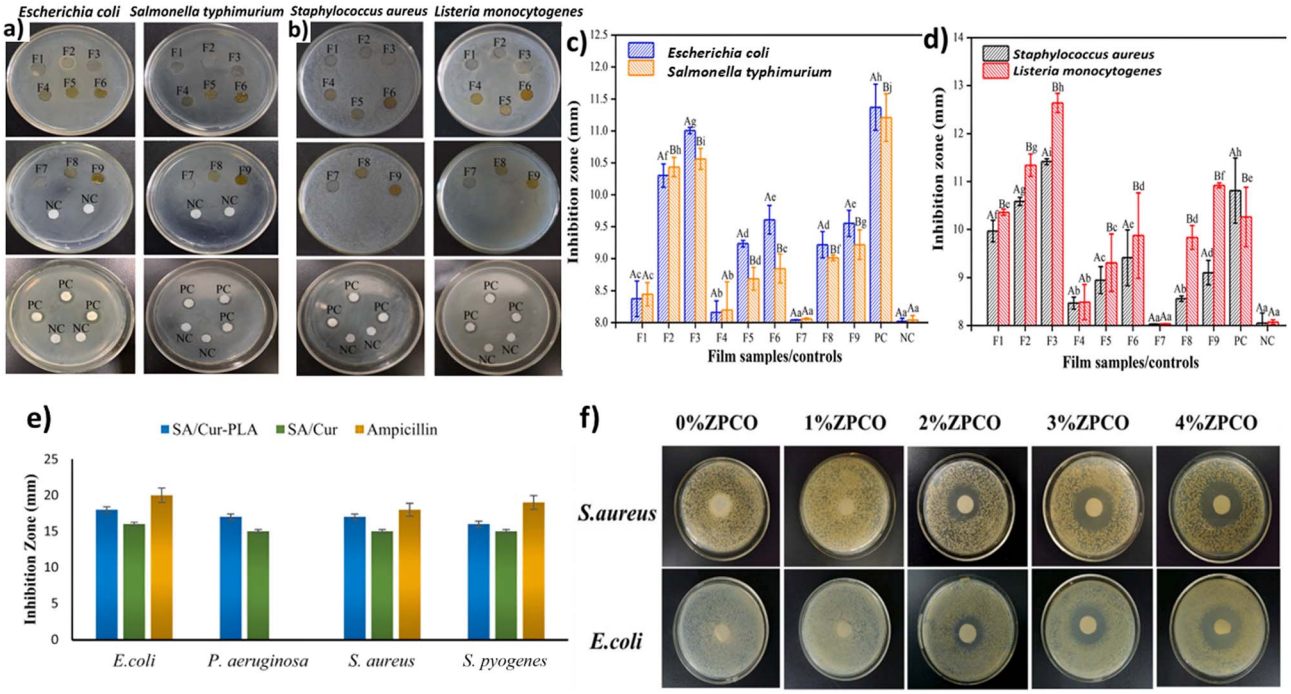

Fig. 7 Antibacterial activity test (a and b) and inhibition zone measurement (c and d) of pectin-based films, reproduced with permission from ref. 116 copyright © 2023 Elsevier Ltd. All rights reserved. (e) Antimicrobial analysis of SA/Cur–PLA, and SA–Cur hydrogel bead, reproduced with permission from ref. 113 copyright © 2023 Elsevier Ltd. All rights reserved. (f) Antimicrobial activity of different concentration of concentration of zein–pectin nanoparticle-stabilized cinnamon essential oil Pickering emulsion (ZPCO) against *Staphylococcus aureus* and *Escherichia coli*, reproduced with permission from ref. 118. Copyright © 2023 Elsevier Ltd. All rights reserved.

antimicrobial nanoparticles has proven effective in inhibiting bacterial growth and extending the shelf life of fresh fruits and vegetables.[123] Its ability to modulate moisture and protect bioactive compounds makes it a viable option for preserving perishable products. Lin *et al.* reported that the incorporation of *Morinda citrifolia* fruit extract significantly enhances the antimicrobial performance of pectin-based films against both Gram-negative and Gram-positive bacteria. The inhibition zones ranged from 9.21 to 11.00 mm against *Escherichia coli*, 8.68 to 10.56 mm against *Salmonella typhimurium*, 8.47 to 11.42 mm for *Staphylococcus aureus*, and 9.30 to 12.64 mm in the case of *Listeria monocytogenes*. The film formulated with 10% extract exhibited the strongest inhibitory effect, a result attributed to its higher concentration of phenolic content, which is known to interfere with bacterial membrane integrity and induce oxidative stress.[124]

One of the main challenges in incorporating plant-derived extracts into polymeric matrices such as pectin is their limited solubility in aqueous environments, which often compromises dispersion uniformity and bioactive efficacy.[125] A promising strategy to overcome this limitation involves the use of Pickering emulsions, which enable the encapsulation and controlled delivery of hydrophobic compounds.[126] In this context, Wu *et al.* demonstrated that chayote tuber starch can be effectively functionalized using a Pickering emulsion system and loaded with cinnamon essential oil in a pectin matrix. The resulting films exhibited strong antimicrobial activity against *Staphylococcus aureus* and *Escherichia coli*, with inhibition zones between 20 and 40 mm, depending on the concentration of zein–pectin nanoparticle-stabilized cinnamon essential oil Pickering emulsion (ZPCO), as illustrated in Fig. 7f. In addition to their antibacterial performance, the films also showed a remarkable enhancement in antioxidant capacity, with DPPH radical scavenging activity increasing from 9% to 60% as the ZPCO content was elevated.[118]

5. Modified biopolymers with nanoparticles

To enhance the antimicrobial properties of CS films, researchers typically incorporate metallic nanoparticles, chiefly silver (AgNPs),[40,41,127,128] and copper- or zinc-oxide nanoparticles (CuONPs and ZnONPs).[129,130] Conventional syntheses employ reducing agents such as $NaBH_4$, NaOH,[41] and sodium citrate; however, these reagents are toxic, costly, or demand harsh conditions, which has driven a shift toward greener alternatives.[131,132] In green routes, bio-molecules (anthocyanins, flavonoids) derived from plants[133] and bacteria[134] simultaneously reduce and stabilize the metal ions. Nanoparticles obtained from biomass sources: shells, leaves, flowers, roots, consequently exhibit broad antibacterial, antifungal, and antiviral activities.[135–138] The four main pathways for metal-ion reduction-plant extracts, bacterial cultures, fungal metabolites and agro-industrial wastes, are summarized in Fig. 8.[139–145] These routes provide both reducing and stabilizing molecules, enabling the

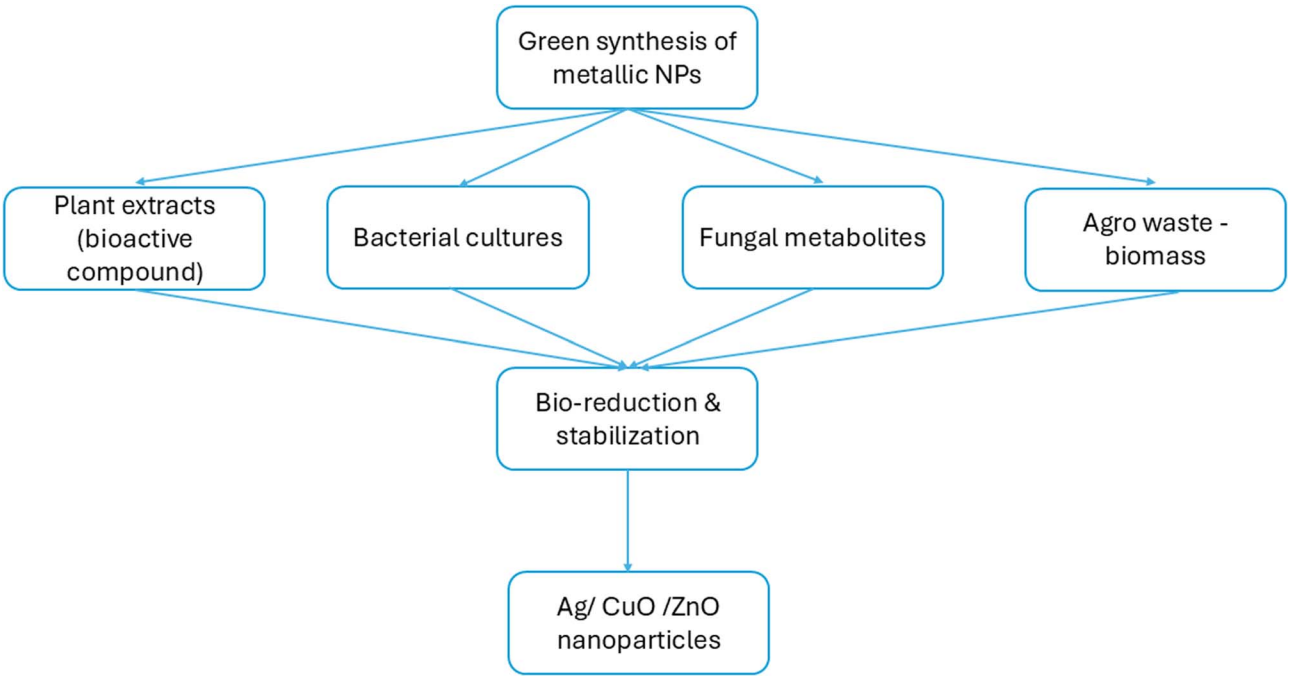

Fig. 8 Green synthesis routes for metallic nanoparticles.

one-step formation of Ag, CuO and ZnO nanoparticles under mild conditions.

Regarding the antimicrobial mechanism of nanoparticles, AgNPs deliver potent, reactive oxygen species (ROS)-mediated killing of *Pseudomonas aeruginosa*, *Bacillus subtilis*, and *Staphylococcus aureus*, along with antioxidant, antipathogenic, and anticholinesterase activities.[146] The underlying steps (Ag^+ binding to the anionic membrane, ROS generation, protein denaturation, and DNA disruption) are illustrated in Fig. 8.[147,148] This broad-spectrum efficacy is largely attributed to their ability to catalyze the generation of ROS and to release Ag^+ ions in a sustained manner. These Ag^+ ions initially interact with the negatively charged microbial cell membrane through coulombic attraction, facilitating their subsequent penetration into the cytoplasm. Once inside the cell, Ag^+ ions react with protein sulfhydryl groups, leading to protein denaturation, inhibition of essential enzymatic activities, and disruption of DNA synthesis. Collectively, these mechanisms result in severe structural and functional cellular damage, ultimately compromising membrane integrity and causing cell death (Fig. 9).[149]

Zhou *et al.* emphasize that AgNPs offer significant advantages over silver ions, mainly due to their controlled and prolonged release.[40] However, they caution against the risks of toxicity at higher doses.[150–157] To address this issue, they proposed the synthesis of an innovative biocomposite composed of a lipopeptide (iturin) with antifungal activity, integrated into a porous CS sponge (see Table 6). This material demonstrated enormous potential as a wound-healing dressing *in vivo*. The synthesis involved mixing CS with an iturin–AgNP solution at concentrations of 0, 5, 10, and 20 μg mL^{-1}. These concentrations influenced the sponge's porosity, water absorption capacity, and morphology. Antibacterial activity was particularly notable at a concentration of 10 μg mL^{-1}, showing effectiveness against *E. coli* and *S. aureus*. Additionally, wound healing tests revealed that this concentration caused no considerable damage to major organs nor left residues. Compared to traditional gauze, the CS sponge dressings exhibited superior physicochemical properties, including higher absorption capacity, appropriate size, and greater ease of use. These attributes resulted in greater efficiency and lower toxicity compared to currently available commercial options.[40]

Similarly, in the work of Zhang and Jiang tea polyphenols (TP) were used to reduce silver ions on chitosan polymer, it is worth notice that TP not only serves as reducing agent, but also as crosslinking agent. To synthesize the composite silver nanoparticles precursors in a fixed mass were mixed with CS and TP at different concentrations (2, 4 and 8 mL of 0.1% (w/v) TP solutions) to obtain CS/TP–AgNP film. In Fig. 10a–d the developed films can be observed, there is an increment in the opacity of the films with the TP addition. From the SEM analysis, small agglomerates are observed with the increment of TP (Fig. 10e–h). When the antibacterial effect of the films was evaluated, *E. coli* and *S. aureus* were used, showing the effectiveness of using AgNPs and TP in CS films, being the most effective for *E. coli*, the film with the highest TP concentration, meanwhile, for *S. aureus* the effect was constant after the addition of 4 mL of TP (Fig. 10i). The CS/TP–AgNP film produced inhibition zones of 22–26 mm against *E. coli* and 18–22 mm against *S. aureus* through combined polycation attraction of CS and Ag-induced ROS that perforate membranes and disrupt DNA replication (Table 7), with efficacy scaling directly with AgNP size (<30 nm) and CS protonation, showing a synergistic interplay between the matrix and the embedded nanoparticles.[127]

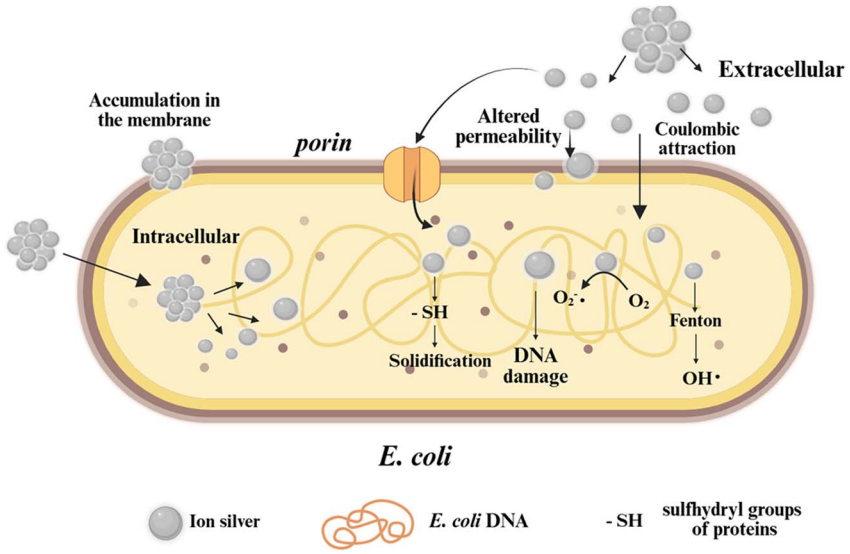

Fig. 9 Proposed mechanism of AgNPs in *E. coli* cells.[147,148]

In a complementary manner, various studies[160,162–164,166,167] highlights the versatility of different forms derived from polymeric compounds, including gels, films, membranes, sponges, spheres, and hydrogels. These materials are specifically designed for applications in coatings intended for the treatment of metabolic, vascular, arterial, and immunosuppressive diseases. Beyond their mechanical and biocompatibility properties, their morphology also plays a critical role in modulating antimicrobial performance. For instance, spherical architecture offers shorter diffusion paths for Ag^+ ions, which can enhance the rate and uniformity of antimicrobial action.[163] In addition, additional mechanisms have been proposed to explain and enhance the antimicrobial behavior of AgNPs. One strategy involves their integration with two-dimensional materials such as MXene, where the nanoparticles function as photothermal enhancers. This also leads to increased generation of ROS, resulting in a synergistic photothermal-oxidative mechanism.[165] Another compelling approach lies in the use of green synthesis routes, especially those employing natural compounds like phenolic terpenes. These molecules contribute to a dual-action antimicrobial mechanism: they disrupt the lipid bilayer by increasing membrane permeability, while simultaneously, Ag^+ ions and ROS induce oxidative stress that impairs cellular respiration by inhibiting key respiratory enzymes.[160]

Dotto *et al.* study emphasizes the potential of natural-origin biomaterials like collagen, chitosan, and gelatin, with particular focus on the advantages of combining gelatin and chitosan. This combination exhibits biological activity, biocompatibility, and water vapor permeability. Moreover, they propose that wound dressings should have key properties, such as antibacterial activity, which can be achieved by impregnating AgNPs. These nanoparticles are synthesized using chitosan as a reducing and stabilizing agent through eco-friendly methodologies. Their study concludes that a concentration of 10 mmol L^{-1} is the most biocompatible, although an increase in nanoparticle concentration affects parameters such as swelling and water vapor permeability, increasing both. Additionally, they confirm that all evaluated concentrations effectively reduce bacterial growth of *Pseudomonas aeruginosa*, when gelatin is blended with chitosan (GCs–AgNP films) the swollen, highly porous network accelerates Ag^+ diffusion; antimicrobial efficacy therefore scales not only with AgNPs dose (10–30 mmol L^{-1}) but also with film porosity/water uptake, giving >4 log reductions for *S. aureus* and *P. aeruginosa* within 6 h.[158]

Beyond films and sponges, Mirda *et al.* highlighted the use of CS as a reducing agent, leveraging its polymeric matrix to minimize metallic nanoparticle aggregation and improve biocompatibility. To synthesize silver–chitosan nanoparticle microspheres (AgNP–chi-spheres), chitosan was dissolved in 1% v/v CH_3COOH, and 2% $AgNO_3$ was gradually added. The resulting solution was dripped into NaOH solutions of varying concentrations (20–50%) using a syringe, followed by washing with ultrapure water and drying (Fig. 11a). SEM images (Fig. 11b) of the AgNP–chi-spheres prepared with 20% NaOH revealed a porous, amorphous surface structure. UV-vis spectroscopy confirmed nanoparticle formation through surface plasmon resonance at 410 nm, though the NaOH concentration influenced the maximum absorbance peak without significantly affecting nanoparticle diameter. XRD analysis demonstrated a crystalline structure with 2θ values of 38.21°, 43.80°, and 57.48°, corresponding to the (111), (200), and (220) planes of AgNPs, with no evidence of silver oxide formation. Antimicrobial testing (Fig. 11c) revealed that AgNP–chi-spheres synthesized with 50% NaOH displayed the most promising results, achieving inhibition zone diameters of 19.5, 18.56, and 12.25 nm for *S. aureus*, *E. coli*, and *C. albicans*, respectively, due to the homogeneous, NaOH-tuned AgNPs ($\approx$47 nm) disrupted membranes while the chitosan shell stabilized ion release.[41]

Although the main asset of AgNPs is their antimicrobial activity, their range of applications is not limited to this field.

Table 6 Characteristics of biopolymers modified with metallic nanoparticles[a]

Material	Biopolymer	NPs	Reducing agent	Reaction conditions	Impregnation	Plasmon (nm)	Form	NPs size (nm)	Ref
CS/TP–AgNPs	Chitosan	Ag	Tea polyphenols (TP)	100 mL of 1 mmol L^{-1} $AgNO_3$ 0.5–8 mL of 0.1% 1 TP, 30 °C, 2 h	AgNPs were mixed in the formed chitosan solution	450	Spherical	28	127
AgNPs–chi-spheres	Chitosan	Ag	NaOH	A chitosan solution (0.2 g of chitosan + 10 mL of 1% (v/v) CH_3COOH) was mixed with 10 mL of 2% $AgNO_3$	*In situ*	410	—	—	41
GCs–AgNPs	Chitosan–gelatin	Ag	Chitosan	60 mmol L^{-1} $AgNO_3$, 90 °C, 21 h	Mixture of 2% (m/v) chitosan with 4% (m/v) gelatin solution and different concentrations of $AgNO_3$	427	—	3–30	158
AgNPs–chitosan	Chitosan	Ag	*Eichhornia crassipes* extract	Mixture of plant extract with $AgNO_3$ solution (0.2 mmol L^{-1}), 1 h	Chitosan 0.5 wt% is mixed with 5% CH_3COOH for 48 h, then taken to 120 °C–4 min and immersed in AgNP solution for 3 days	425–445	Spherical round	39.44–103.8	159
CS–AgNP	Chitosan	Ag	*L. reuteri* cells	—	Mixture of 10 mL of *L. reuteri* cells with chitosan (chitosan with CH_3COOH) and $AgNO_3$ solution (1 mmol L^{-1}) for 48 h	415	Quasi-spherical	40–90	134
(Pam/Cs)–AgNP	Chitosan	Ag	Gamma radiation	5–15 kGy with a dose rate of 1 kGy h^{-1}	Irradiation of chitosan at 5 kGy and subsequent mixing with 1% glacial CH_3COOH and acrylamide at 70 °C–24 h. Then it is mixed with $AgNO_3$ for 24 h and irradiated with gamma rays	—	—	16.4–71	132
PVA–CTS–Ag	Chitosan	Ag	Glucose	2% chitosan is mixed with $AgNO_3$ and glucose at 95 °C for 6 h	4 g of the CTS–Ag NP colloidal solution was mixed with 6 g of 8% by weight PVA solution and the electrospun fiber mats were obtained using electrospinning equipment	420	—	~32	160
PVA:CS:SS–AgNP	Chitosan	Ag	*Cynodon dactylon* leaf extract	Mixing *Cynodon dactylon* leaf extract with $AgNO_3$ at 80 °C for 15 min	Mixture of PVA, CS and silk serine in different proportions for 4 h, then AgNPs are added	434	Spherical	9.2–24.2	131
Alg@AgNPs	Alginate	Ag	Alginate	$AgNO_3$ is mixed with alginate, the mixture is at 60 °C for 24 h, then precipitated with acetone, filtered and pulverized		—	—	9–21	161
Cs/AgNPs	Chitosan	Ag	Aloe vera gel extract	Mixture of $AgNO_3$ with aloe vera extract at 80 °C	0.5% chitosan with CH_3COOH is mixed with different concentrations of AgNP	400–500	Spherical	100 ± 40	162

Table 6 (*Contd.*)

Material	Biopolymer	NPs	Reducing agent	Reaction conditions	Impregnation	Plasmon (nm)	Form	NPs size (nm)	Ref
CHI–Eos–AgNPs	Chitosan	Ag	Tyrosine	A solution of tyrosine is boiled, then mixed with $AgNO_3$ and KOH.	The glacial CH_3COOH solution was mixed with glycerol for 24 h, then the essential oil was incorporated for 24 h and finally the AgNPs were incorporated with 5% weight under stirring for 24 h	420	—	—	163
CH/Au@sMX	Chitosan	Au	Sodium citrate solution (1%)	Chloroauric acid is mixed with boiling sodium citrate solution for 15 min	The composite sponges were manufactured by a typical cross-linking method	525	Spherical	24	164
Chi–SNCs-spheric	Chitosan	Ag	Chitosan	Under vigorous stirring of $AgNO_3$ with a chitosan solution for 15 h	The chitosan–nanoparticle solution is dripped into NaOH, using a micropipette	410	Spherical	4.3–5.8	165
CH–GE–AgNPs	Chitosan–gelatin	Ag	*M. frondosa* leaf extract	The *M. frondosa* leaf extract is mixed at 80 °C for 1 h	Chitosan (dissolved CH_3COOH), 2% gelatin, AgNPs and polyethylene glycol are mixed and left at room temperature until evaporation	426	Triangular and quasi-spherical	10–30	166
PSG–CuZn films	Starch	CuO ZnO	Bacterium, *Stenotrophomonas maltophilia*	100 mL sterile Luria Bertani broth. The broth was inoculated with 1 mL of 18 h old culture of *S. maltophilia*, incubated at 30 °C, 150 rpm, 24 h + 2 mmol L^{-1} of $CuSO_4$ or $ZnSO_4$ solution was added, pH = 8, 3 days	CuO nanoparticles (15 mg) or ZnO nanoparticles (25 mg) dissolved in 100 μL DI water were added to PSG to form the PSG–Cu film, and PSG–Zn polymer film. Respectively	254 for CuO NPs 600 for ZnO NPs	Roughly spherical	—	130
Chitosan–CuO NPs films	Chitosan	CuO	Leaf extract (10% w/v) of sting nettle (*Urtica dioica* L.)	The nettle extract (10% v/v) was added dropwise to a solution of $CuSO_4$	Chitosan (1% w/v) + CH_3COOH (1% v/v) was mixed with NPs	320 for CuO NPs	—	10–50 for CuO NPs	129
Chitosan–ZnO NPs films		ZnO		0.01 mol L^{-1} pH = 7 or Zn $(CH_3COOH)_2$ 0.01 mol L^{-1}, pH = 9	The chitosan–NP composite films were developed by casting techniques to form films	330 for ZnO NPs		50–100 for ZnO NPs	
Iturin–AgNPs-based CS composite sponge	Chitosan	Ag	Iturin	2 mL of iturin 1 mg mL^{-1} + $AgNO_3$ 0.1 mg mL^{-1} + UV radiometer (λ = 365 nm) at 5 cm, for 30 min	Chitosan 1 g + CH_3COOH (1% v/v) was mixed with different concentration of iturin–AgNPs. Deposited in a polystyrene well plate, frozen at −80 °C, 1 h, followed by lyophilization for 24 h, then treated with 2% NaOH (w/w) solution 2 h	450	Spherical	20 ± 10	40

[a] CS/TP–AgNPs: chitosan/tea polyphenols–silver nanoparticles composite film, AgNPs–chi-spheres: silver nanoparticles–chitosan composite particles sphere, GCs–AgNPs: chitosan/gelatin–silver nanoparticles, AgNPs–chitosan: silver nanoparticles–chitosan, CS–AgNP: chitosan–silver nanoparticles, (Pam/Cs)–AgNP: silver nanoparticles-loaded hydrogel nanocomposites of acrylamide/chitosan, PVA–CTS–Ag: poly(vinyl alcohol)–chitosan–silver nanoparticles PVA:CS:SS–AgNP: polyvinyl alcohol:chitosan:silk sericin:silver nanoparticles, Alg@AgNPs: alginate@silver nanoparticles, Cs/AgNPs: chitosan/silver nanoparticles, CHI–Eos–AgNPs: chitosan based films–essential oils–AgNPs, CH/Au@sMX: chitin/gold nanoparticles@sMX, Chi–SNCs-spheric: chitosan–silver–nanocomposite-sphere, CH–GE–AgNPs: chitosan/gelatin/silver nanoparticles, PSG–CuZn films: composites of PVA–starch–glycerol with CuO and ZnO, chitosan–CuO NPs films: chitosan–CuO nanoparticles, chitosan–ZnO NPs films: chitosan–ZnO nanoparticles.

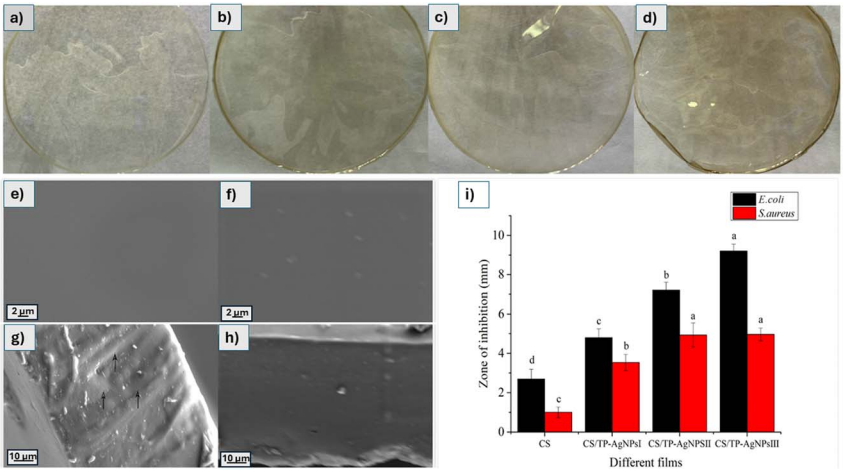

Fig. 10 (a) CS film, (b) CS/TP–AgNPsI film, (c) CS/TP–AgNPsII film, (d) CS/TP–AgNPsIII film. SEM images of the surface and cross-section for (e and g) CS film and (f and h) CS/TP–AgNPsIII film. (i) The inhibition zone (A) of chitosan films, both with and without varying concentrations of TP–AgNPs, against the growth of *E. coli* and *S. aureus*. Error bars represent the standard deviation, reproduced with permission from ref. 127 copyright © 2019 Elsevier B.V. All rights reserved.

Another potential use is demonstrated by Ahmad, R., and Ansari, K. in the synthesis of a bio-nanocomposite (Alg@AgNPs) for use as an adsorbent. Their approach considers biocompatibility and green chemistry during the AgNP synthesis process, utilizing alginate as a reducing and stabilizing agent (Fig. 12a–c). Adsorption tests indicate that the Langmuir model is the most suitable, with a desorption value exceeding 83% (Fig. 12d), indicating that the composite can be successfully regenerated for up to four cycles.[161]

With these advancements, green methodologies not only involve the use of non-toxic compounds or solvents but also promote the utilization of several types of waste, such as agricultural, industrial, or technological residues, as raw materials or as reducing and stabilizing agents in the synthesis of nanomaterials, including metallic nanoparticles. For instance, Mondal *et al.* propose the synthesis of AgNPs (Fig. 13a–c) through an innovative approach that combines green synthesis using aqueous extracts from water hyacinth leaves (*Eichhornia crassipes*) with silver particles previously treated with HNO_3, obtained from electronic waste such as motherboards, circuits, and PCB boards. Furthermore, their study explores the extraction of biopolymers from shrimp shells. These materials are used to coat cotton fabrics, evaluating both their antimicrobial activity (Fig. 13d–g), which showed positive results within a pH range of 7 to 12, and their physical properties. Physical tests revealed remarkable wrinkle recovery, along with slight increases in weight, thickness, and tensile strength.[159]

As Ag, CuO and ZnO nanoparticles are recognized to have good antimicrobial properties.[168,169] In the study of Francis *et al.*, they incorporated these nanoparticles in PVA–starch–glycerol (PSG). PVA have been used to improve the mechanical properties of biopolymers;[170–173] as is the case of cellulose[174] and starch,[130,175–177] and glycerol is used as plasticizer.[178] First, the authors prepared CuONPs and ZnONPs using a bacterium, *Stenotrophomonas maltophilia* using sterile Luria Bertani broth.[179–182] The Cu and Zn sulphates precursors were added in total concentration of 2 mmol L^{-1}. The successful CuONPs and ZnONPs biosynthesis was confirmed by DRX. The SEM images showed spherical nanoparticles. The PSG films were prepared by mixing a PVA solution with starch, and glycerol solutions. After that, a dispersion of CuONPs, ZnONPs and CuONPs + ZnONPs were added to the PSG films to form PSG–Cu, PSG–Zn, and PSG–CuZn films, respectively. The reaction took place for 30 min at 95 °C. Then the formed films were added to glass plates and dried for 24 h at 50 °C. The SEM image of the PSG film exhibited a clear surface (Fig. 14a).

Fig. 14b–d shows the SEM images of PSG with CuO, PSG with ZnO, and PSG with CuONPs and ZnONPs, respectively, where the metal nanoparticles embedded in the polymer were distinctly visible, making the surface appear textured. The antifungal activity of CuONPs and ZnONPs was evaluated against *Aspergillus niger*, *Aspergillus calidoustus*, and *Penicillium chrysogenum*, which were previously isolated from spoiled fruits and vegetables. The nanoparticles were applied at varying concentrations (1, 3, and 5 μg for CuO; 5, 7, and 10 μg for ZnO) on potato dextrose agar plates inoculated with fungal spores, followed by incubation at 30 °C for 24 h. The results showed a concentration-dependent inhibition of fungal growth, with larger zones of inhibition (ZOIs) observed at higher nanoparticle concentrations. Among the fungi, all three were sensitive to CuO nanoparticles, whereas *A. niger* exhibited resistance to ZnO nanoparticles. Positive controls using $CuSO_4$ and $ZnSO_4$ at equivalent concentrations showed no antifungal activity, highlighting the specific effectiveness of the nanoparticles. The minimal inhibitory concentration (MIC) and minimal fungicidal concentration (MFC) for CuO and ZnO nanoparticles were both 1 μg mL^{-1}, which was notably lower than the 2 μg mL^{-1} required for amphotericin B.

The antifungal activity was visually and quantitatively assessed. The ZOI data, as depicted in Fig. 14e, showed a marked increase in fungal inhibition with higher nanoparticle concentrations, with CuO demonstrating superior antifungal

Table 7 Antimicrobial properties of biopolymers modified with nanoparticles: mechanisms of action, influencing factors, and target pathogens[a]

Material	Antimicrobial pathogens	Assay	Antimicrobial mechanisms	Main factors that influence the antimicrobial efficacy	Ref.
CS/TP–AgNPs	*S. aureus* and *E. coli*	Paper disk diffusion	Electrostatic interaction by chitosan and ROS-mediated membrane disruption by AgNPs	AgNP dose/size; chitosan protonation (pH)	127
AgNPs–chi-spheres	*S. aureus*, *E. coli* and *C. albicans*	Diffusion	AgNPs damage membranes; chitosan stabilizes NPs	NaOH concentration (particle homogeneity)	41
GCs–AgNPs	*Staphylococcus aureus*; *Pseudomonas aeruginosa*	Agar-plate CFU reduction	Ag^+ release & ROS generation	AgNPs concentration; swelling/porosity of the GCs network	158
AgNPs–chitosan	*S. aureus* and *E. coli*	Disc diffusion	Synergistic Ag^+/ROS attack plus chitosan's polycationic interaction with cell envelopes	AgNP loading (100–400 μg); contact time	159
CS–AgNP	*Bacillus subtilis*; *E. coli*	Paper-disc diffusion	ROS-mediated membrane disruption from AgNPs	AgNPs dose; particle size	134
(Pam/Cs)–AgNP	*Candida albicans*	CFU mL^{-1}	—	CS content; AgNP loading	132
PVA–CTS–Ag	*S. aureus*; *E. coli*	Disc diffusion	Ag^+/ROS plus chitosan electrostatic interaction	Relative PVA/CTS ratio; AgNP wt%	160
PVA:CS:SS–AgNP	*E. coli*; *S. aureus*	Disc diffusion	—	CS/sericin fraction and concentration, and AgNP inclusion	131
Cs/AgNPs	*S. aureus*; *P. aeruginosa*, *C. albicans*	Agar-well diffusion	Ag^+ ions-mediated cell disruption	NP size; Ag content	162
CHI–EOs–AgNPs	*E. coli*; *L. monocytogenes*; *S. typhimurium*; *A. niger*	log CFU reduction on food-contact films	Combined cell-wall disruption by oregano/cinnamon essential-oil phenolics and Ag^+-induced ROS	EO concentration; AgNP level; storage time	163
CH/Au@sMX	*S. aureus*; *E. coli*	Plate-count (sponge contact)	MXene sharp-edge physical cutting plus Au-NP photothermal/ROS effects	sMX (MXene) weight%; Au loading; exposure time	164
Chi–SNCs-spheric	*S. aureus*; *P. aeruginosa*	Agar-well diffusion	Ultra-small AgNPs (≈4 nm), release ions and generate ROS; chitosan sphere increases local NP density	NPs homogeneity (NaOH in synthesis); size of NPs, chitosan degree of deacetylation	165
CH–GE–AgNPs	*E. coli*; *S. aureus*; *S. mutans*, *P. aeruginosa*, *C. albicans*	Disc diffusion	Bactericidal activity: Ag^+/ROS Antifungal activity: AgNPs-mediated membrane degradation	AgNPs concentration level (0.0025–0.01% w/w); film density/thickness	166
PSG–CuZn films	*Aspergillus niger*, *Aspergillus calidoustus*, *Penicillium chrysogenum*	Diffusion	—	CuONPs and ZnNPs concentration	130
Chitosan–CuO NPs films Chitosan–ZnO NPs films	*Enterobacter cloacae* MTCC 509, *Salmonella typhii*, *Staphylococcus aureus*, and *Campylobacter jejuni*	Disk diffusion	ROS + ion release	NP dispersion; dosage	129
Iturin–AgNPs-based CS composite sponge	*E. coli* and *S. aureus*	Disk diffusion	Ion release	Iturin–AgNP load; porosity	40

[a] ZOI: nanoparticles zone of inhibition.

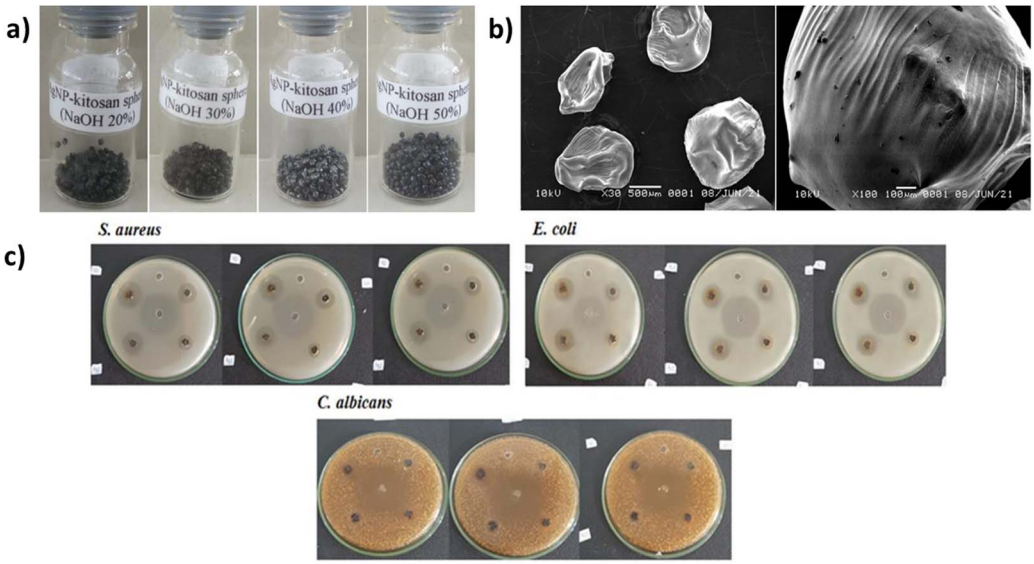

Fig. 11 (a) Products (b) SEM spectrum (c) antimicrobial activity against *S. aureus*, *E. coli*, and *C. albicans* of AgNPs-chi-spheres reproduced with permission from ref. 41 copyright © 2021. Licensee MDPI, under the terms and conditions of the CC BY license.

efficacy compared to ZnO. Fig. 14f and g provided visual evidence of antifungal activity, with clear ZOIs observed on agar plates treated with CuO and ZnO nanoparticles. Additionally, polymer films embedded with these nanoparticles (PSG–Cu and PSG–CuZn) exhibited significant antifungal effects, particularly against *A. niger* and *A. calidoustus*, outperforming amphotericin B in some cases. In particular, the CuO/ZnO-loaded films (PSG–CuZn) rely primarily on redox cycling and metal-ion leaching. These pathways are exceptionally lethal to fungal hyphae; complete growth suppression of *A. niger* was achieved at 25 mg L^{-1} Cu/Zn (1 : 1) in a PVA–starch–glycerol matrix. These findings underscore the potential of CuONPs and ZnONPs, especially when incorporated into biodegradable polymer films, as effective antifungal agents for applications in food preservation and packaging.[130] These findings underscore the potential of CuONPs and ZnONPs, especially when incorporated into

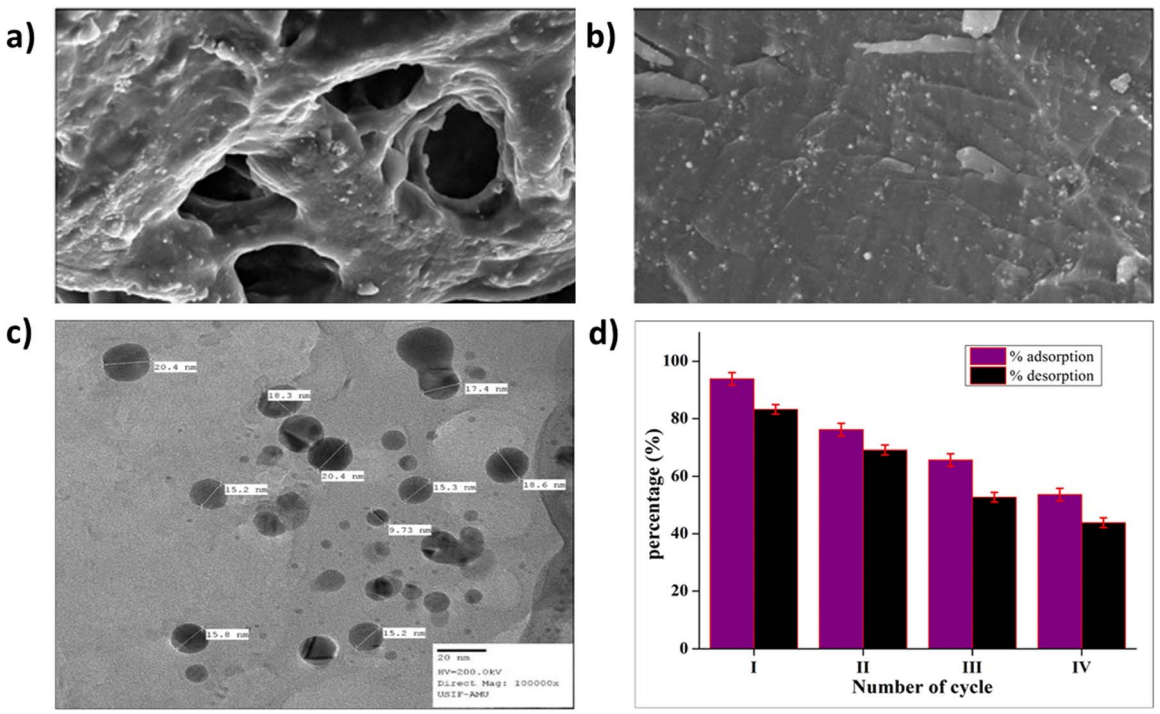

Fig. 12 SEM images of (a) before adsorption and (b) after adsorption of crystal violet (CV) dye, (c) TEM of Alg@AgNPs and (d) regeneration cycles for CV dye on Alg@AgNPs, reproduced from ref. 161 copyright © 2022 published by Elsevier B.V.

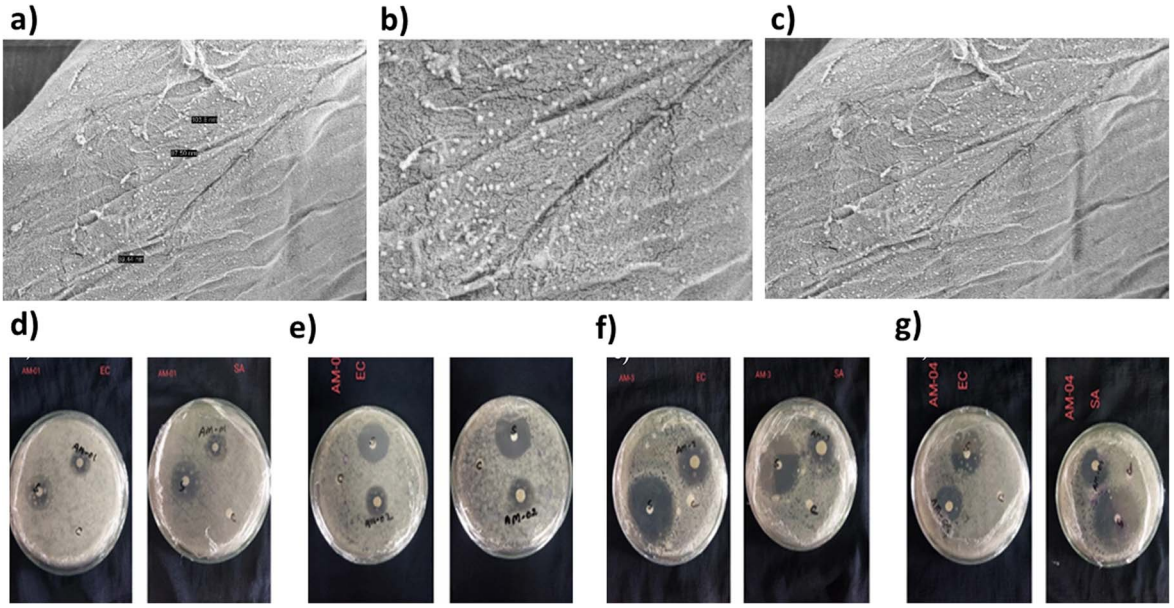

Fig. 13 SEM images of AgNPs: (a) nanoparticle (NP) size, (b) green synthesis, (c) chemical synthesis, inhibition zone of AgNPs, (d) recycled AgNPs in green synthesis, (e) pure AgNPs in green synthesis, (f) recycled AgNPs in chemical synthesis, and (g) pure AgNPs in chemical synthesis on fabric samples against *S. aureus* and *E. coli*. Reproduced from ref. 159 copyright © 2023, The Author(s) under a Creative Commons Attribution 4.0.

biodegradable polymer films, as effective antifungal agents for applications in food preservation and packaging.[130]

Kalia *et al.* utilized polyphenolic compounds from the *Urtica dioica* leaves to synthesize CuONPs and ZnONPs, acting as reducing and stabilizing agents. These nanoparticles were subsequently incorporated into a nanocomposite matrix of chitosan and acetic acid. Physical-chemical analyses, including UV-vis, SEM, and EDS, revealed the surface plasmon resonance, shape, size, and quantitative presence of metallic compounds. The ZnO–chitosan nanomaterial showed a reduction in moisture content and solubility due to nanoparticle intercalation with the matrix. Conversely, CuO–chitosan films exhibited enhanced antioxidants and antimicrobial properties, proving effective in extending the shelf life and quality of fruits. Both metallic oxide NPs were active against enteric pathogens (*E. cloacae*, *S. typhii*). The film generated 16–18 mm zones, driven by Cu^{2+}/Zn^{2+} leaching; dispersion quality determined potency.[129]

Structural modifications, synthesis techniques, and applications of nanometric materials derived from chitosan (CS) have been widely reported. Preliminary studies suggest that combining CS and nanoparticles yields more effective bactericidal and antimicrobial agents, targeting pathogens such as *Escherichia coli*, *Acinetobacter baumannii*, *Staphylococcus aureus*, *Candida* spp., *Pseudomonas* sp., *Aspergillus niger*, *Penicillium* sp., *Enterococcus faecalis*, *Pseudomonas aeruginosa*, and *Streptococcus pneumonia*.[35,159,161,168,169] Collectively, these findings evidence that tailoring NP physicochemistry together with matrix functionality is essential for designing bio–NPs composites that deliver potent, broad-spectrum antimicrobial performance without compromising biocompatibility.

In conclusion, biopolymer–nanoparticle composites represent a powerful platform for antimicrobial materials, but their design must consider multiple physicochemical and biological factors to optimize efficacy across a broad spectrum of pathogens. The incorporation of green synthesis techniques, controlled nanoparticle distribution, and functional synergistic agents (*e.g.*, polyphenols, essential oils, iturin) is essential for advancing safe, sustainable, and effective antimicrobial technologies.

6. Application of interest of biopolymer–nanoparticle composites

Preliminary studies on the synthesis of nanoparticle-enhanced biopolymers have generated increasing interest across different industrial sectors, mainly due to their biocompatibility and broad multifunctional properties. In this context, Fernandes *et al.*, described four key principles that explain the interaction between polymers and nanoparticles: (i) improved nanoparticle adhesion through non-covalent interactions, (ii) increased multifunctionality, (iii) the ability to act as an *in situ* reducing agent, and (iv) provision of structural support.[183] These features have been particularly applied in the textile industry, where advanced fabrics are being developed to block pathogen transmission, neutralize odors, prevent skin irritation, and enhance user protection.[184–187]

One example of this approach was reported by Che *et al.*, who synthesized a hyperbranched polymer, EPDA-HBP (derived from epichlorohydrin, dimethylamine, and amino-HBP), applied it to cotton fabric, and generated AgNPs *in situ*. This dual-functional method ensured stable NPs fixation, reaching a loading of 180 mg Ag per kg of fiber and achieving more than 90% bacterial reduction against *S. aureus* and *E. coli*, even after 30 washing cycles.[188]

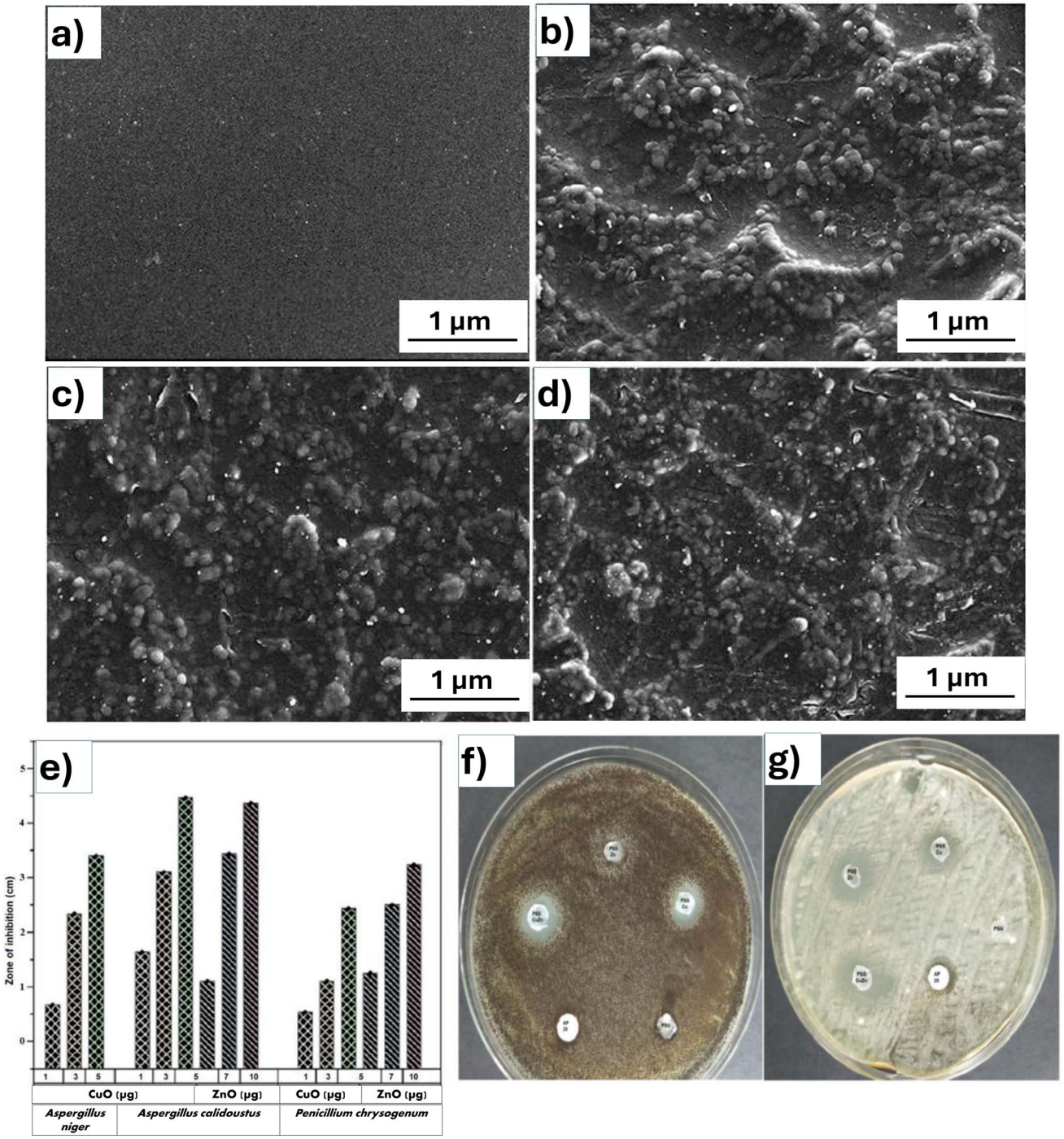

Fig. 14 SEM images of (a) PSG, (b) PSG–Cu, (c) PSG–Zn, and (d) PSG–CuZn films. (e) The zone of inhibition (ZOI) exhibited by CuO and ZnO nanoparticles against *Aspergillus niger*, *Aspergillus calidoustus*, and *Penicillium chrysogenum* at concentrations of 1, 3, and 5 μg for CuO nanoparticles and 5, 7, and 10 μg for ZnO nanoparticles. (f) Antifungal activity of PSG, PSG–Cu, PSG–Zn, PSG–CuZn, and amphotericin B (20 μg) against *Aspergillus niger*. (g) Antifungal activity of PSG, PSG–Cu, PSG–Zn, PSG–CuZn, and amphotericin B (20 μg) against *Aspergillus calidoustus* reproduced with permission from ref. 130 copyright © 2022 by the authors. Licensee MDPI, under the terms and conditions of the CC BY license.

Another common strategy involves depositing thin polymer/nanoparticle films onto cotton, polyester, or cotton–polyester blends. Polymeric matrices such as poly(vinyl alcohol) (PVA), carboxymethylcellulose (CMC), or CS are combined with AgNPs or ZnNPs to form composite coatings. These systems enhance color, improve UV shielding, provide antimicrobial activity against *E. coli*, *S. aureus*, and *C. albicans*, and increase mechanical performance compared to untreated fabrics. The choice of polymer is an important factor; for instance, CS facilitates better nanoparticle dispersion and stability, achieving microbial reduction rates above 83%.[189]

Gao *et al.* proposed a complementary two-step process. First, AgNPs were immobilized on the fabric using a polydopamine adhesive layer; this was followed by a hydrophobic overlayer made from materials such as polydimethylsiloxane, polyimide, CS, hexamethyldisiloxane, PEDOT:PSS, or chitosan–organosilica (Cs–OSH). This configuration provided the textile with self-cleaning properties, resistance to acidic and alkaline conditions, antibacterial activity (*E. coli*, *S. aureus*), superhydrophobicity (water contact angle up to 150°), and high electrical conductivity (>1076 S m^{-1} after 120 min of treatment).[184–186,190] Lastly, some alternatives involve a plasma pre-treatment on polyester fabrics, which facilitates the formation of functional groups (–COO, –OO–) that enhance AgNP impregnation. This process not only boosts antimicrobial performance but also provides hydrophobic properties (contact angle of 151.1°) and electrical conductivity (0.6860 S cm^{-1}).[190,191]

The food industry has consistently focused on improving food safety by extending product shelf life, ensuring quality, and minimizing waste. In this pursuit, natural biopolymers, particularly CS, have shown significant potential. Derived from chitin, CS exhibits antimicrobial, antioxidant, and bioactive properties, making it a promising candidate for food preservation and packaging applications. Its effectiveness has been widely documented, especially in meat and fresh products, where it helps extend shelf life. For example, Tuesta *et al.* reported advancements in the development of chitosan-based materials, highlighting their sustainability and functional performance in food packaging systems.[192] However, biopolymers such as CS still present intrinsic limitations, including low mechanical strength, high gas permeability, and limited thermal stability. To address these challenges, researchers have explored the incorporation of metallic and inorganic nanoparticles, which offer unique advantages such as high surface-area-to-volume ratios and strong antimicrobial and antioxidant activity. Nanomaterials including ZnO, TiO_2, CuO, AgNPs, and AuNPs have been successfully integrated into polymeric matrices, significantly enhancing their overall functionality.[193] As a result, the combination of nanoparticles with biopolymers has led to the development of nano-reinforced biocomposites, which not only improve the structural properties of the material but also provide additional functionalities. Among the most studied systems is the incorporation of ZnONPs into CMC films, combined with grape seed extract, which has been shown to effectively inhibit lipid oxidation and suppress the growth of psychrotrophic bacteria.[194] Likewise, AgNPs have demonstrated strong antimicrobial performance and significantly extend the shelf life of fruits and vegetables, while TiO_2NPs are known to enhance the mechanical and thermal stability of biopolymer matrices. The synergistic combination of CuONPs with cellulose nanofibers has also proven effective in reducing moisture permeability and inhibiting microbial growth. Finally, AuNPs, due to their inert, non-toxic nature and catalytic properties, are considered multifunctional materials with potential not only in antimicrobial packaging systems but also as sensors for detecting foodborne contaminants.

In the biomedical field, particularly in the treatment and prevention of various diseases, systems based on biopolymers combined with nanoparticles have shown promising potential. A representative example is the study by Boca *et al.* who developed phototherapeutic agents for cancer treatment using silver nanotriangles coated with chitosan. These nanostructures exhibited higher cancer cell mortality rates compared to gold nanorods coated with thiolated polyethylene glycol. The therapeutic effect relies on localized heating at the tumor site, generated by light-to-heat conversion through surface plasmon resonances, with strong absorption in the near-infrared (NIR) region at 724 nm. Additionally, the system showed a zeta potential of +39 mV, which was associated with enhanced cellular uptake and good biocompatibility.[195]

Alternatively, several studies have focused on the development of hydrogels composed of metallic nanoparticles (Ag or Au) and biopolymers such as chitosan, poly(vinyl alcohol), carboxymethylcellulose, poly(lactic-*co*-glycolic acid), polyethylene glycol, or polyvinylpyrrolidone, with or without the inclusion of active pharmaceutical ingredients (*e.g.*, doxorubicin or paclitaxel). These systems have demonstrated efficacy against melanoma, lung cancer, prostate cancer (PC3 cell line), and breast cancer (MCF-7), and also exhibited antimicrobial activity against Gram-positive and Gram-negative bacteria.[196–198] In all cases, a synergistic effect was observed, with nanoparticle concentration and chitosan content being key factors in the antitumor activity.[199]

While conventional chemical synthesis methods remain widely used, green synthesis routes have also been proposed. Metallic nanoparticles have been synthesized using plant extracts such as *Camellia sinensis* (green tea) and *Moringa oleifera* and subsequently incorporated into polymeric matrices including poly(vinyl alcohol) (PVA), polyethylene glycol (PEG), and polylactide-based polypropylene. In some cases, additional compounds such as *S*-nitrosoglutathione (GSNO) were added to enhance the therapeutic effect.[200] These formulations showed strong antibacterial activity against both Gram-positive and Gram-negative strains, along with significant reductions in the viability of human cancer cell lines including cervical (HeLa), prostate (PC3), and glioblastoma (A172). This anticancer effect has been associated with the combined action of the nanoparticles and the bioactive compounds present in the plant extracts used as reducing agents.[201]

7. Challenges in the large-scale production, of biopolymer–nanoparticle composites, toxicity, and regulatory approvals

To address the issue of large-scale production, we have incorporated insights from Muñoz-Bonilla *et al.* who highlighted that despite the promising antimicrobial properties of biopolymer-based materials, their translation to industrial-scale applications remains limited due to cost, reproducibility, and scalability constraints in synthesis and processing methods.[202]

Concerning nanoparticle toxicity, we acknowledge that our earlier emphasis on biocompatibility might have lacked sufficient nuance. As highlighted by Altaf *et al.* although polysaccharide-based nanoparticles like chitosan, starch, and

alginate are generally considered non-toxic and biodegradable, their behavior in complex biological or environmental systems can vary significantly depending on particle size, surface modification, and synthesis route. This variability underscores the importance of case-specific toxicity assessments.[203]

Regarding regulatory approvals, Ruan *et al.* explicitly point out that the long-term antimicrobial performance of polysaccharide-based systems under physiological conditions is still under investigation and that regulatory acceptance remains a significant bottleneck for clinical and food-related applications. The lack of harmonized standards and long-term safety data complicates the approval process for these advanced materials.[202]

Overall, the synergy between biopolymers and metallic nanoparticles represents a promising frontier for the development of next-generation multifunctional materials. However, to fully harness their potential, future research must address critical challenges related to large-scale production, long-term biocompatibility, and regulatory approval frameworks. Special attention should be given to developing standardized protocols for green synthesis and toxicity assessment, which are essential for the safe translation of these materials into clinical and food-related environments. Moreover, the design of smart biopolymer–nanoparticle systems with stimuli-responsive behaviors and tunable degradation profiles could unlock new applications in targeted drug delivery, active packaging, and environmental remediation. Interdisciplinary collaboration among material scientists, toxicologists, and regulatory bodies will be vital to accelerate the adoption of these technologies and ensure their sustainable and responsible integration into real-world applications.

8. Environmental implications of biopolymer–nanoparticle composites: sustainability and biodegradability considerations

The integration of nanoparticles into biopolymer matrices has garnered significant attention for enhancing material performance, particularly in sectors such as packaging,[204,205] agriculture,[204,206] and biomedical applications.[207,208] However, this technological advancement also introduces complexities in evaluating environmental sustainability, particularly through Life Cycle Assessment (LCA) methodologies. Fig. 15 provides a schematic overview of the integration of nanoparticles into biopolymer matrices, highlighting their potential benefits, associated environmental burdens identified through LCA, and strategies for reconciling performance with sustainability.

Biopolymers are often viewed as sustainable alternatives to petroleum-based plastics due to their renewable origins and potential for biodegradability. Nevertheless, the incorporation of inorganic nanoparticles into these matrices can alter their environmental footprint in multifaceted ways.[209,210] While nanoparticles can improve barrier properties, mechanical strength, and antimicrobial activity, leading to potential reductions in material use and food waste, their production, functionalization, and end-of-life behavior can generate significant environmental burdens.[210,211]

LCA studies have demonstrated that even small mass fractions of nanoparticles (based on carbon, for example carbon nanotubes, graphene, carbon black) can significantly increase the non-renewable energy use and greenhouse gas emissions of biopolymer–nanoparticle composites.[210,212] On the other hand, for NPs containing layered double hydroxide nanoparticles it was observed in the study of Schrijvers *et al.* that the lowest environmental impact was reached for the materials containing the LDHs compared with the pristine polymer.[213] The synthesis of biopolymer–nanoparticle composites with nanoparticles generates an increment of cost production even though when nanoparticles are the minor component.[210] In addition, the type and synthesis route of nanoparticles determine the overall environmental cost. Particularly, AgNPs, widely used for their antimicrobial properties, contribute substantially to the environmental impact in biopolymers composite production, with over 90% of their lifecycle impacts attributed to upstream silver production.[214]

Methods like flame spray pyrolysis further exacerbate these effects due to high electricity consumption and low yields.[214] Since AgNPs present the non-renewable energy use, they have a high Global Warning Potential (GWP).[210] To justify the inclusion of metallic nanoparticles in biopolymers, functionality-based LCA approaches are recommended. These models compare materials not just by mass or composition but by their performance outcomes, such as shelf-life extension or weight reduction. For example, in the work of Zhang *et al.*[211] demonstrated that a hybrid system of Ag and TiO_2 nanoparticles at reduced loadings provided the same antimicrobial efficacy as higher individual concentrations, leading to lower environmental burdens. Similarly, functionalized nanoparticles, although more resource-intensive to produce, can enhance dispersion and interfacial compatibility, thereby improving the overall performance and reducing material needs.[215]

Biopolymer matrices typically biodegrade under controlled composting or anaerobic digestion, releasing carbon dioxide or methane in a theoretically net-neutral carbon cycle.[216,217] However, the presence of inorganic nanoparticles complicates this picture. These fillers are not biodegradable and may persist in the environment's post-polymer degradation. Their fate, transformation, and potential toxicity in natural ecosystems remain areas of active research.[218] Moreover, concerns over nanoparticle migration from packaging materials into food, and subsequently into the human body, raise questions not only about human health but also about environmental accumulation. Regulatory frameworks (*e.g.*, EC regulation no. 10/2011 and 2020/1245) have begun addressing these concerns, yet global harmonization is lacking.[219,220]

Although biopolymers are often biodegradable, recycling remains a desirable pathway to reduce environmental impact. Some nanocomposite systems, such as those incorporating clay or metallic fillers, demonstrate good recyclability and reuse potential.[221] As an example, using chitosan (Chi), and poly(vinyl alcohol) (PVA) as a matrix for loading TiO_2NPs, and the chlorophyll (Chl) as a natural light photocatalyst, provided the new, and efficient photocatalyst (PVA/TiO_2/Chi/Chl). TiO_2NPs and chlorophyll were applied to modify the PVA/Chi and use as an

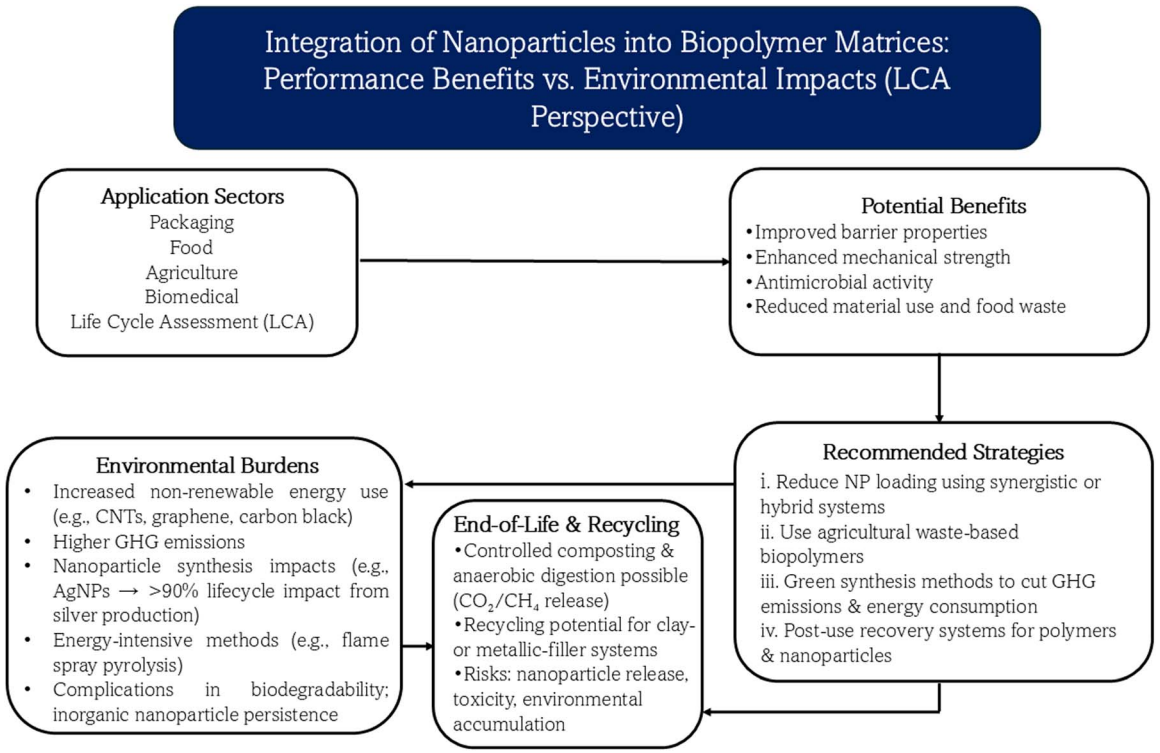

Fig. 15 Flowchart illustrating the integration of nanoparticles into biopolymer matrices, summarizing the key application sectors, potential performance benefits (*e.g.*, improved barrier properties, mechanical strength, and antimicrobial activity), environmental burdens identified through Life Cycle Assessment (LCA) (*e.g.*, increased non-renewable energy use, greenhouse gas emissions, and complications in biodegradability), and proposed strategies to reconcile enhanced functionality with environmental sustainability.

effective nano-photocatalyst for degradation of methylene blue (MB), 4-chlorophenol (4-CP), and Congo Red (CR) for the first time, which showed efficiently promoted the separation of electron–hole pairs to enhance the photocatalytic activity. The degradation of MB was examined in the presence and absence of visible light. Also, the various contact times and the synergic effect of the different components of the bionanocomposite were studied. The high efficiency (96%) was achieved under visible-light irradiation (LED lamp 70 W by λ is 425 nm) at 60 min. The present bionanocomposite was identified by FT-IR spectra, field-emission scanning electron microscopy (FE-SEM) image, XRD pattern, energy-dispersive X-ray (EDX), and photoluminescence (PL) analyses. Also, the antibacterial properties of PVA/TiO_2/Chi/Chl as a distinctive feature were examined by the agar disk diffusion and colony counter method. The zone of inhibition for both *S. aureus* and *E. coli* bacteria were around 2.08 ($\pm$0.02), and 1.98 ($\pm$0.02), respectively. The colony counter was checked in the presence and the absence of visible light. Bacterial contamination presents serious risks to human health, therefore the prominent antimicrobial capability bionanocomposite inhibits the growth of both *S. aureus*, and *E. coli* bacteria under LED light irradiation.

The use of green, and available materials, easy synthetic processes, simple extraction method, eco-friendly protocols, high removal efficiency, and noticeable antibacterial properties are advantageous to work.[3] Nevertheless, repeated processing must not lead to nanoparticle release or loss of functional properties. To reconcile the performance benefits with environmental sustainability we can consider (i) reducing nanoparticle loading by leveraging synergistic effects or hybrid systems to maintain functionality at lower concentrations.[211] (ii) Using agricultural waste-based biopolymers to avoid land-use conflicts and enhance circularity. (iii) Developing green synthesis methods for nanomaterials to minimize GHG emissions and energy consumption. (iv) Implementing post-use recovery systems for both polymers and nanoparticles to reduce persistence and toxicity in the environment.

9. Conclusions

Polysaccharide-based biopolymer–nanoparticle composites hold significant promise as multifunctional materials for antimicrobial applications. However, despite their inherent biocompatibility and biodegradability, emerging evidence indicates that their toxicity profiles can vary widely depending on synthesis parameters and environmental context. This underscores the necessity of conducting case-specific safety evaluations. Moreover, regulatory hurdles remain a major barrier to clinical and commercial deployment, primarily due to the absence of standardized evaluation protocols and long-term performance data. To fully realize the potential of these materials, future research should prioritize the development of green synthesis routes, robust toxicity assessment frameworks, and stimuli-responsive systems with tunable degradation.

Interdisciplinary efforts among researchers, toxicologists, and regulators will be essential to bridge existing gaps and facilitate the safe, scalable, and responsible integration of these composites into biomedical, food, and environmental applications.

Despite these advancements, challenges remain in optimizing large-scale production, ensuring consistent nanoparticle dispersion within biopolymer matrices, and assessing long-term biocompatibility. Additionally, addressing concerns regarding nanoparticle toxicity and achieving regulatory approvals are critical steps before their widespread application in medical and food-related fields.

Future research should focus on developing scalable and cost-effective green synthesis strategies while ensuring the safety and stability of biopolymer–nanoparticle composites. Advances in nanotechnology, such as the design of hybrid nanostructures with controlled release mechanisms, could further enhance the functionality of these materials. Moreover, exploring new bio-based reducing agents and crosslinking techniques may lead to improved mechanical and barrier properties. Overall, the synergy between biopolymers and nanoparticles presents promising opportunities for next-generation materials with enhanced performance in diverse applications. Sustained interdisciplinary collaboration among materials scientists, chemists, biotechnologists, and regulatory experts will be essential in unlocking the full potential of these innovative composites.

Abbreviations

AHP	Alkaline hydrogen peroxide
AMCC	Antimicrobial microcrystalline cellulose
ASC	Acidified sodium chlorite
ASTM	American Society of Testing and Materials
AgNPs	Silver nanoparticles
AgNP–chi-spheres	Silver–chitosan nanoparticle microspheres
Alg@AgNPs	Alginate@silver nanoparticles
AP	Apple pectin
BC	Bacterial cellulose
BNC	Bacterial nanocellulose
BLO	Alginate extracted from blades of *Laminaria ochroleuca*
BSP	Alginate extracted from of *Saccorhiza polyschides*
CA	Commercial alginate
Ca-alginate-hydrogels	Calcium (+2)-alginate hydrogels
CEC	Chemically extracted chitosan
CEO	Cinnamon essential oil
Chitosan/PVA	Chitosan/PVA-based film
CH/Au@sMX	Chitin/gold nanoparticles@sMX
CHI–Eos–AgNPs	Chitosan-based films–essential oils–AgNPs
Chi–SNCs-spheric	Chitosan–silver–nanocomposite-sphere
Chitosan–CuO NPs films	Chitosan–CuO nanoparticles
CH–GE–AgNPs	Chitosan/gelatin/silver nanoparticles
CNCs	Cellulose nanocrystals
CuONPs	Copper oxide
CS	Chitosan
CS-C	Commercial chitosan
Cs/AgNPs	Chitosan/silver nanoparticles
CS/TP–AgNPs	Chitosan/tea polyphenols–silver nanoparticles composite film
CK	Plastic film
CP	Chitosan–polyvinyl alcohol Film
CPB	Chitosan–polyvinyl alcohol–bacterial cellulose film
$CPB_{0.8}$	Chitosan–polyvinyl alcohol–bacterial cellulose film loaded with 0.8% ginger essential oil
DE	Degree of esterification
DD	Deacetylation degree
DSC	Differential scanning calorimetry
DPPH	2,2-Difenil-1-picrilhidrazilo
DWS	Dewaxed wheat straw
DWS_{ASC}	Cellulose isolated *via* alkaline hydrogen peroxide treatment
DWS_{ASC}	Cellulose isolated *via* acidified sodium chlorite treatment
EEC	Enzymatically extracted chitosan
EDS	Energy dispersive X-ray spectroscopy
FBC	Fat binding capacity
FTIR	Fourier transform infrared spectroscopy
Fe-NTA	Ferric nitrilotriacetate
Gal-A	Galacturonic acid
G	α-L-Guluronate
GCs–AgNPs	Chitosan/gelatine–silver nanoparticles
GPS	Gel permeation chromatography
HCl	Hydrochloric acid
HPLC	High-performance liquid chromatography
HPP	High-pressure processing
HRE	Heating reflux extraction
^{1}H NMR	Proton nuclear magnetic resonance
LCNFs	Lignocellulosic nanofibrils
LMP	Low methoxy pectin
M	β-D-Mannuronate
MAE	Microwave assisted extraction
MeO	Methoxyl content
MBC	Minimum bactericidal concentration
MIC	Minimum inhibitory concentration
MW	Molecular weight
NaOH	Sodium hydroxide
ROS	Reactive oxygen species
TEMPO	(2,2,6,6-Tetramethylpiperidin-1-yl)oxyl
TP	Tea polyphenols
TGA	Thermogravimetric analysis
TVB-N	Total volatile basic nitrogen
PC	Positive control
PEG	Polyethylene glycol
(Pam/Cs)–AgNP	Silver nanoparticles-loaded hydrogel nanocomposites of acrylamide/chitosan
PSG	PVA–starch–glycerol
PSG–CuZn films	Composites of PVA–starch–glycerol with CuO and ZnO

PVA	Polyvinyl alcohol
PVA:CS:SS–AgNP	Polyvinyl alcohol:chitosan:silk sericin:silver nanoparticles
PVA–CTS–Ag	Poly(vinyl alcohol)–chitosan–silver nanoparticles
SA/Cur	Sodium alginate–curcumin hydrogel
SA/Cur–PLA	Sodium alginate–curcumin–polylactic acid hydrogel
SEM	Scanning electron microscopy
SLO	Alginate extracted from stipes of *Laminaria ochroleuca*
SSP	Alginate extracted from stipes of *Saccorhiza polyschides*
sMX	Ultrasound-assisted extraction
UF	Ultrafiltered
WBC	Water binding capacity
WRP	Watermelon rind pectin
wt%	Weight percentage
MXene	Synthesized by the method LiF/HCl
UAE	Ultrasound assisted extraction
UAEP	Ultrasound extracted citrus pectin
XRD	X-ray diffraction
ZnONPs	Zin oxide nanoparticles
ZPCO	Zein–pectin nanoparticle-stabilized cinnamon essential oil Pickering emulsion
ZOI	Larger zones of inhibition

Author contributions

Roxana Yesenia Pastrana Alta: writing – original draft. Emily Huarote-Garcia: writing – original draft. Miguel Adolfo Egusquiza Huamani: writing – original draft. Angélica M. Baena-Moncada: writing – review & editing, supervision, investigation, conceptualization.

Conflicts of interest

There are no conflicts to declare.

Data availability

No primary research results, software or code have been included and no new data were generated or analysed as part of this review.

Acknowledgements

This research work was financially supported by Funding Program No. PE501082481-2023-PROCIENCIA, in the framework of the call for Basic and Applied Research Projects.

References

1 R. K. Gond, M. K. Gupta and M. Jawaid, *Polym. Compos.*, 2021, **42**, 5400–5412.
2 L. Montes, M. Gisbert, I. Hinojosa, J. Sineiro and R. Moreira, *Carbohydr. Polym.*, 2021, **272**, 118455.
3 S. Rakshit, K. Pal, S. Mondal, A. Jana, K. C. Mondal and S. K. Halder, *Int. J. Biol. Macromol.*, 2023, **244**, 125389.
4 L. Wang, Z. Zhao, H. Zhao, M. Liu, C. Lin, L. Li and B. Ma, *Food Hydrocolloids*, 2022, **122**, 107061.
5 M. Bustamante-Torres, B. Arcentales-Vera, J. Estrella-Nuñez, H. Yánez-Vega and E. Bucio, *Macromol*, 2022, **2**, 258–283.
6 J. Baranwal, B. Barse, A. Fais, G. L. Delogu and A. Kumar, *Polymers*, 2022, **14**, 983.
7 F. Hadjkacem, J. Elleuch, M. Aitouguinane, F. Chakou, A. V. Ursu, P. Dubessay, N. Bourgougnon, M. Traikia, D. Le Cerf, Z. El Alaoui-Talibi, C. El Modafar, Z. Boual, M. D. O. El Hadj, C. Delattre, G. Christophe, P. Michaud, I. Fendri, S. Abdelkafi and G. Pierre, *Int. J. Biol. Macromol.*, 2023, **253**, 126757.
8 Z. Li, A. Liu, H. Wu, A. Naeem, Q. Fan, Z. Jin, H. Liu and L. Ming, *Int. J. Biol. Macromol.*, 2024, **254**, 127890.
9 J.-W. Rhim, H.-M. Park and C.-S. Ha, *Prog. Polym. Sci.*, 2013, **38**, 1629–1652.
10 I. J. Joye and D. J. McClements, *Curr. Opin. Colloid Interface Sci.*, 2014, **19**, 417–427.
11 G. Guan, L. Zhang, J. Zhu, H. Wu, W. Li and Q. Sun, *J. Hazard. Mater.*, 2021, **402**, 123542.
12 V. De Matteis, M. Cascione, D. Costa, S. Martano, D. Manno, A. Cannavale, S. Mazzotta, F. Paladini, M. Martino and R. Rinaldi, *J. Mater. Res. Technol.*, 2023, **24**, 1015–1033.
13 J. Liu, J. Huang, Z. Hu, G. Li, L. Hu, X. Chen and Y. Hu, *Int. J. Biol. Macromol.*, 2021, **189**, 363–369.
14 V. G. L. Souza, M. M. Alves, C. F. Santos, I. A. C. Ribeiro, C. Rodrigues, I. Coelhoso and A. L. Fernando, *Coatings*, 2021, **11**, 646.
15 S. Yousefiasl, H. Manoochehri, P. Makvandi, S. Afshar, E. Salahinejad, P. Khosraviyan, M. Saidijam, S. Soleimani Asl and E. Sharifi, *J. Nanostruct. Chem.*, 2023, **13**, 389–403.
16 M. K. Rasweefali, S. Sabu, K. V. Sunooj, A. Sasidharan and K. A. M. Xavier, *Carbohydr. Polym. Technol. Appl.*, 2021, **2**, 100032.
17 V. Bello and O. Olafadehan, *Alex. Eng. J.*, 2021, **60**, 3869–3899.
18 Ö. Y. Öğretmen, B. Karsli and E. Çağlak, *J. Agric. Sci.*, 2022, **28**, 490–500.
19 M. Triunfo, E. Tafi, A. Guarnieri, R. Salvia, C. Scieuzo, T. Hahn, S. Zibek, A. Gagliardini, L. Panariello, M. B. Coltelli, A. De Bonis and P. Falabella, *Sci. Rep.*, 2022, (12), 1–17.
20 F. Jiang, X. Li, Y. Duan, Q. Li, Y. Qu, G. Zhong, M. Qiu, J. Zhang, C. Zhang and X. Pan, *Colloids Surf., B*, 2023, **222**, 113030.
21 C. Molina-Ramírez, P. Mazo, R. Zuluaga, P. Gañán and J. Álvarez-Caballero, *Polymers*, 2021, **13**, 2079.
22 Y. Zhang, Y. Wang, Z. Zhang, W. Cui, X. Zhang and S. Wang, *J. Environ. Chem. Eng.*, 2021, **9**, 104647.
23 C. Burgos-Díaz, M. Opazo-Navarrete, J. L. Palacios, T. Barahona, Y. Mosi-Roa, F. Anguita-Barrales and M. Bustamante, *Polymers*, 2021, **13**, 2304.

24 B. Sudatta, V. Sugumar, R. Varma and P. Nigariga, *Int. J. Biol. Macromol.*, 2020, **163**, 423–430.
25 B. Taser, H. Ozkan, A. Adiguzel, T. Orak, M. O. Baltaci and M. Taskin, *Int. J. Biol. Macromol.*, 2021, **183**, 1191–1199.
26 A. M. Sixto-Berrocal, M. Vázquez-Aldana, S. P. Miranda-Castro, M. A. Martínez-Trujillo and M. R. Cruz-Díaz, *Int. J. Biol. Macromol.*, 2023, **230**, 123204.
27 Q. Dong, W. Qiu, Y. Feng, Y. Jin, S. Deng, N. Tao and Y. Jin, *eFood*, 2023, **4**, e73.
28 E. Y. Wardhono, M. P. Pinem, I. Kustiningsih, M. Effendy, D. Clausse, K. Saleh and E. Guénin, *Carbohydr. Polym.*, 2021, **267**, 118180.
29 D. Vallejo-Domínguez, E. Rubio-Rosas, E. Aguila-Almanza, H. Hernández-Cocoletzi, M. Ramos-Cassellis, M. Luna-Guevara, K. Rambabu, S. Manickam, H. S. H. Munawaroh and P. L. Show, *Ultrason. Sonochem.*, 2021, **72**, 105417.
30 A. Ewais, R. A. Saber, A. Abdel Ghany, A. Sharaf and M. Sitohy, *SN Appl. Sci.*, 2023, **5**, 1–19.
31 I. Donati and S. Paoletti, in *Alginates: Biology and Applications*, Springer, 2009, pp. 1–53.
32 H. Kim, S. Kang, K. Li, D. Jung, K. Park and J. Lee, *Int. J. Biol. Macromol.*, 2021, **169**, 122–129.
33 O. Maikovych, P. Pasetto, N. Nosova, O. Kudina, D. Ostapiv, V. Samaryk and S. Varvarenko, *Gels*, 2025, **11**, 174.
34 A. M. Signori, K. d. O. Santos, R. Eising, B. L. Albuquerque, F. C. Giacomelli and J. B. Domingos, *Langmuir*, 2010, **26**, 17772–17779.
35 K. Kasemets, J. Laanoja, M. Sihtmäe, H. Vija, I. Kurvet, M. Otsus and A. Kahru, *Proceedings*, 2023, **92**, 40.
36 N. Basavegowda and K.-H. Baek, *Polymers*, 2021, **13**, 4198.
37 Y. Liu, H. Shan, C. Zeng, H. Zhan and Y. Pang, *Materials*, 2022, **15**, 4909.
38 L.-S. Wang, C.-Y. Wang, C.-H. Yang, C.-L. Hsieh, S.-Y. Chen, C.-Y. Shen, J.-J. Wang and K.-S. Huang, *Int. J. Nanomed.*, 2015, 2685–2696.
39 D. Gangadharan, K. Harshvardan, G. Gnanasekar, D. Dixit, K. M. Popat and P. S. Anand, *Water Res.*, 2010, **44**, 5481–5487.
40 L. Zhou, X. Zhao, M. Li, L. Yan, Y. Lu, C. Jiang, Y. Liu, Z. Pan and J. Shi, *Int. J. Biol. Macromol.*, 2021, **181**, 1183–1195.
41 E. Mirda, R. Idroes, K. Khairan, T. E. Tallei, M. Ramli, N. Earlia, A. Maulana, G. M. Idroes, M. Muslem and Z. Jalil, *Polymers*, 2021, **13**, 3990.
42 T. Hahn, J. Egger, S. Krake, M. Dyballa, L. Stegbauer, N. von Seggern, I. Bruheim and S. Zibek, *J. Appl. Polym. Sci.*, 2024, **141**, e54789.
43 M. Derraz, A. Elouahli, C. Ennawaoui, M. A. Ben Achour, A. Rjafallah, E. M. Laadissi, H. Khallok, Z. Hatim and A. Hajjaji, *J. Compos. Sci.*, 2023, **7**, 260.
44 G. Hao, Y. Hu, L. Shi, J. Chen, A. Cui, W. Weng and K. Osako, *Sci. Rep.*, 2021, **11**, 1–9.
45 I. B. Amor, H. Hemmami, S. E. Laouini, H. B. Temam, H. Zaoui and A. Barhoum, *World J. Microbiol. Biotechnol.*, 2023, **39**, 1–12.
46 L. A. Picos-Corrales, A. M. Morales-Burgos, J. P. Ruelas-Leyva, G. Crini, E. García-Armenta, S. A. Jimenez-Lam, L. E. Ayón-Reyna, F. Rocha-Alonzo, L. Calderón-Zamora, U. Osuna-Martínez, A. Calderón-Castro, G. De-Paz-Arroyo and L. N. Inzunza-Camacho, *Polymers*, 2023, **15**, 526.
47 S. G. Kou, L. Peters and M. Mucalo, *Carbohydr. Polym.*, 2022, **282**, 119132.
48 H. Hemmami, I. Ben Amor, S. Zeghoud, A. Ben Amor, S. E. Laouini, A. Alsalme, D. Cornu, M. Bechelany and A. Barhoum, *Front. Chem.*, 2024, **12**, 1353524.
49 S. Krake, C. Conzelmann, S. Heuer, M. Dyballa, S. Zibek and T. Hahn, *Biotechnol. Bioprocess Eng.*, 2024, **29**, 942–954.
50 S. S. Fernando, C. Jo, D. C. Mudannayake and D. D. Jayasena, *Carbohydr. Polym.*, 2024, **324**, 121477.
51 L. A. Rodrigues, I. Radojčić Redovniković, A. R. C. Duarte, A. A. Matias and A. Paiva, *ACS Omega*, 2021, **6**, 28729–28741.
52 H. Hemmamı, I. B. Amor, A. B. Amor, S. Zeghoud, S. Ahmed and A. A. Alhamad, *J. Turk. Chem. Soc., Sect. A*, 2024, **11**, 341–364.
53 K. Li, Z. Guo, X. Chen, J. Wang, A. El-Araby, L. E. Ghadraoui and F. Errachidi, *Molecules*, 2022, **27**, 8285.
54 F. Hisham, M. H. Maziati Akmal, F. Ahmad, K. Ahmad and N. Samat, *Ain Shams Eng. J.*, 2024, **15**, 102424.
55 M. B. d. O. Silva, S. A. de Oliveira, D. dos and S. Rosa, *J. Clean. Prod.*, 2024, **440**, 140726.
56 K. Mohan, A. R. Ganesan, P. N. Ezhilarasi, K. K. Kondamareddy, D. K. Rajan, P. Sathishkumar, J. Rajarajeswaran and L. Conterno, *Carbohydr. Polym.*, 2022, **287**, 119349.
57 A. Saravanan, P. S. Kumar, D. Yuvaraj, S. Jeevanantham, P. Aishwaria, P. Gnanasri, M. Gopinath and G. Rangasamy, *Environ. Res.*, 2023, **221**, 115306.
58 J. Wang and S. Zhuang, *J. Clean. Prod.*, 2022, **355**, 131825.
59 H. Bojorges, A. Martínez-Abad, M. Martinez-Sanz, M. D. Rodrigo, F. Vilaplana, A. López-Rubio and M. J. Fabra, *Carbohydr. Polym.*, 2023, **299**, 120175.
60 H. Bojorges, A. López-Rubio, A. Martínez-Abad and M. J. Fabra, *Trends Food Sci. Technol.*, 2023, **140**, 104142.
61 L. Cao, W. Lu, A. Mata, K. Nishinari and Y. Fang, *Carbohydr. Polym.*, 2020, **242**, 116389.
62 I. M. Savić Gajić, I. M. Savić, A. M. Ivanovska, J. D. Vunduk, I. S. Mihalj and Z. B. Sviračev, *Mar. Drugs*, 2024, **22**, 280.
63 S. Kaidi, F. Bentiss, C. Jama, K. Khaya, Z. Belattmania, A. Reani and B. Sabour, *Colloids Interfaces*, 2022, **6**, 51.
64 A. Nesic, M. V. De Bonis, G. Dal Poggetto, G. Ruocco and G. Santagata, *Polymers*, 2023, **15**, 2979.
65 N. J. Borazjani, M. Tabarsa, S. G. You and M. Rezaei, *Int. J. Biol. Macromol.*, 2017, **101**, 703–711.
66 A. Mohammed, A. Rivers, D. C. Stuckey and K. Ward, *Carbohydr. Polym.*, 2020, **245**, 116419.
67 A. Benslima, S. Sellimi, M. Hamdi, R. Nasri, M. Jridi, D. Cot, S. Li, M. Nasri and N. Zouari, *Food Biosci.*, 2021, **40**, 100873.
68 P. Torabi, N. Hamdami and J. Keramat, *Sep. Sci. Technol.*, 2022, **57**, 872–885.
69 A. Malvis Romero, F. Brozio, S. Kammler, C. Burkhardt, L. Baruth, M. Kaltschmitt, G. Antranikian and A. Liese, *Chem. Ing. Tech.*, 2023, **95**, 549–556.
70 N. T. K. Tran, V. B. Nguyen, T. Van Tran and T. T. T. Nguyen, *Food Chem.*, 2023, **418**, 135807.

71 M. Spinei and M. Oroian, *Int. J. Biol. Macromol.*, 2023, **224**, 739–753.
72 T. Qi, J. Ren, X. Li, Q. An, N. Zhang, X. Jia, S. Pan, G. Fan, Z. Zhang and K. Wu, *Carbohydr. Polym.*, 2023, **309**, 120682.
73 D. A. Méndez, M. J. Fabra, L. Gómez-Mascaraque, A. López-Rubio and A. Martinez-Abad, *Foods*, 2021, **10**, 738.
74 D. Panwar, P. S. Panesar and H. K. Chopra, *Food Biosci.*, 2023, **51**, 102231.
75 C. S. Shivamathi, S. Gunaseelan, M. R. Soosai, N. S. Vignesh, P. Varalakshmi, R. S. Kumar, S. Karthikumar, R. V. Kumar, R. Baskar and S. P. Rigby, *Food Hydrocolloids*, 2022, **123**, 107141.
76 F. Zhang, L. Zhang, J. Chen, X. Du, Z. Lu, X. Wang, Y. Yi, Y. Shan, B. Liu, Y. Zhou, X. Wang and X. Lü, *Food Chem.*, 2022, **368**, 130833.
77 M. Yu, Y. Xia, M. Zhou, Y. Guo, J. Zheng and Y. Zhang, *Carbohydr. Polym.*, 2021, **258**, 117662.
78 Z. Li, B. Zhou, T. Zheng, C. Zhao, Y. Gao, W. Wu, Y. Fan, X. Wang, M. Qiu and J. Fan, *Foods*, 2023, **12**, 423.
79 W. S. Abou-Elseoud, E. A. Hassan and M. L. Hassan, *Carbohydr. Polym. Technol. Appl.*, 2021, **2**, 100042.
80 H. Chen, Y. Liu, J. Zhang, Y. Jiang and D. Li, *Int. J. Biol. Macromol.*, 2022, **221**, 976–985.
81 O. Y. Alothman, L. K. Kian, N. Saba, M. Jawaid and R. Khiari, *Ind. Crops Prod.*, 2021, **159**, 113075.
82 A. Kumar, V. Gupta and K. K. Gaikwad, *Biomass Convers. Biorefin.*, 2023, **13**(17), 1–8.
83 M. Rizwan, S. R. Gilani, A. I. Durrani and S. Naseem, *Int. J. Biol. Macromol.*, 2021, **191**, 964–972.
84 S. P. Bangar, P. Kajla and T. Ghosh, *Int. J. Biol. Macromol.*, 2023, **227**, 762–776.
85 R. S. Abolore, S. Jaiswal and A. K. Jaiswal, *Carbohydr. Polym. Technol. Appl.*, 2024, **7**, 100396.
86 U. Qasim, Z. Ali, M. S. Nazir, S. Ul Hassan, S. Rafiq, F. Jamil, A. H. Al-Muhtaseb, M. Ali, M. B. Khan Niazi, N. M. Ahmad, S. Ullah, A. Mukhtar and S. Saqib, *Adv. Polym. Technol.*, 2020, **2020**, 9765950.
87 A. B. Perumal, R. B. Nambiar, P. S. Sellamuthu, E. R. Sadiku, X. Li and Y. He, *Chemosphere*, 2022, **287**, 132084.
88 N. A. M. Razali, R. M. Sohaimi, R. N. I. R. Othman, N. Abdullah, S. Z. N. Demon, L. Jasmani, W. M. Z. W. Yunus, W. M. H. W. Ya'acob, E. M. Salleh, M. N. Norizan and N. A. Halim, *Polymers*, 2022, **14**, 387.
89 C. J. Huntley, K. D. Crews, M. A. Abdalla, A. E. Russell and M. L. Curry, *Int. J. Chem. Eng.*, 2015, **2015**, 658163.
90 S. Huang, X. Liu, C. Chang and Y. Wang, *Cellulose*, 2020, **27**, 2991–3011.
91 P. Shahbazi, T. Behzad and P. Heidarian, *Wood Sci. Technol.*, 2017, **51**, 1173–1187.
92 M. A. Shamsabadi, T. Behzad and R. Bagheri, *Fibers Polym.*, 2015, **16**, 579–584.
93 A. Alemdar and M. Sain, *Bioresour. Technol.*, 2008, **99**, 1664–1671.
94 C. Zhong, C. Wang, F. Huang, H. Jia and P. Wei, *Carbohydr. Polym.*, 2013, **94**, 38–45.
95 H. Li, H. Zhang, L. Xiong, X. Chen, C. Wang, C. Huang and X. Chen, *Fibers Polym.*, 2019, **20**, 975–981.
96 Y. Lu, Q. He, G. Fan, Q. Cheng and G. Song, *Green Process. Synth.*, 2021, **10**, 779–804.
97 Q. Liu, W. Q. He, M. Aguedo, X. Xia, W. B. Bai, Y. Y. Dong, J. Q. Song, A. Richel and D. Goffin, *Carbohydr. Polym.*, 2021, **253**, 117170.
98 W. J. J. Huijgen, G. Telysheva, A. Arshanitsa, R. J. A. Gosselink and P. J. de Wild, *Ind. Crops Prod.*, 2014, **59**, 85–95.
99 A. Kumar, V. Gupta and K. K. Gaikwad, *Biomass Convers. Biorefin.*, 2023, **13**, 1–8.
100 D. Divakaran, I. Suyambulingam, M. Sanjay, V. Raghunathan, V. Ayyappan and S. Siengchin, *Int. J. Biol. Macromol.*, 2024, **254**, 127687.
101 A. C. F. Louis, S. Venkatachalam and S. Gupta, *Ind. Crops Prod.*, 2022, **179**, 114695.
102 H. M. Shaikh, A. Anis, A. M. Poulose, S. M. Al-Zahrani, N. A. Madhar, A. Alhamidi and M. A. Alam, *Polymers*, 2021, **13**, 1893.
103 R. M. Cherian, A. Tharayil, R. T. Varghese, T. Antony, H. Kargarzadeh, C. J. Chirayil and S. Thomas, *Carbohydr. Polym.*, 2022, **282**, 119123.
104 R. M. Sheltami, I. Abdullah, I. Ahmad, A. Dufresne and H. Kargarzadeh, *Carbohydr. Polym.*, 2012, **88**, 772–779.
105 G. M. Oprică, D. M. Panaitescu, B. E. Lixandru, C. D. Uşurelu, A. R. Gabor, C.-A. Nicolae, R. C. Fierascu and A. N. Frone, *Pharmaceutics*, 2023, **15**, 2672.
106 N. P. Mangalagiri, S. K. Panditi and N. L. L. Jeevigunta, *Heliyon*, 2021, **7**(4), e06835.
107 H. Abral, A. B. Pratama, D. Handayani, M. Mahardika, I. Aminah, N. Sandrawati, E. Sugiarti, A. N. Muslimin, S. M. Sapuan and R. A. Ilyas, *Int. J. Polym. Sci.*, 2021, **2021**, 6641284.
108 L. Stasiak-Różańska, A. Berthold-Pluta, T. Aleksandrzak-Piekarczyk, A. Koryszewska-Bagińska and M. Garbowska, *Polymers*, 2024, **16**, 2316.
109 H. S. El-Sayed, S. M. El-Sayed, A. M. M. Mabrouk, G. A. Nawwar and A. M. Youssef, *J. Polym. Environ.*, 2021, **29**, 1941–1953.
110 L. O. Xavier, W. G. Sganzerla, G. B. Rosa, C. G. da Rosa, L. Agostinetto, A. P. d. L. Veeck, L. C. Bretanha, G. A. Micke, M. Dalla Costa, F. C. Bertodi, P. L. M. Barreto and M. R. Nunes, *Int. J. Biol. Macromol.*, 2021, **169**, 183–193.
111 M. Duan, J. Sun, Y. Huang, H. Jiang, Y. Hu, J. Pang and C. Wu, *Food Sci. Hum. Wellness*, 2023, **12**, 614–621.
112 X. Chen, W. Lan and J. Xie, *Food Chem.*, 2024, **441**, 138343.
113 M. Paswan, A. K. Singh Chandel, N. I. Malek and B. Z. Dholakiya, *Int. J. Biol. Macromol.*, 2024, **254**, 128005.
114 M. Abdin, M. Mabrouk, L. El-Sebaiy, M. Eissa, M. El-Bana, M. A. Salama, A. E. El-Beltagy and M. A. Naeem, *Int. J. Biol. Macromol.*, 2023, **240**, 124474.
115 R. Jafari, M. Zandi and A. Ganjloo, *J. Polym. Environ.*, 2023, **31**, 1568–1583.
116 X. Lin, S. Chen, R. Wang, C. Li and L. Wang, *Food Hydrocolloids*, 2023, **134**, 108025.
117 S. Shivangi, D. Dorairaj, P. S. Negi and N. P. Shetty, *Food Hydrocolloids*, 2021, **121**, 107046.

118 H. Wu, J. Wang, T. Li, Y. Lei, L. Peng, J. Chang, S. Li, X. Yuan, M. Zhou and Z. Zhang, *Int. J. Biol. Macromol.*, 2023, **240**, 124444.
119 S. Zhang, B. Gatsi, X. Yao, Y. Jin and H. Amhal, *Carbohydr. Polym.*, 2025, **352**, 123189.
120 S. Pereira, A. Costa-Ribeiro, P. Teixeira, L. Rodríguez-Lorenzo, M. Prado, M. A. Cerqueira and A. Garrido-Maestu, *Polymers*, 2023, **15**, 3759.
121 Y. El Atki, I. Aouam, F. El Kamari, A. Taroq, K. Nayme, M. Timinouni, B. Lyoussi and A. Abdellaoui, *J. Adv. Pharm. Technol. Res.*, 2019, **10**, 63–67.
122 L. T. Maswanganye, S. K. Pillai and D. Sivakumar, *Coatings*, 2025, **15**, 105.
123 S. B. Dlala, Z. Mzoughi, M. I. Dammak, K. Khwaldia, D. Le Cerf, H. B. Halima, N. Jaffrezic-Renault, H. Korri-Youssoufi and H. Majdoub, *Process Biochem.*, 2025, 56–64.
124 F. Obeng-Boateng, S. W. Kpordze and F. Addy, *PLoS One*, 2024, **19**, e0313003.
125 F. Baghi, S. Ghnimi, G. Agusti, E. Dumas and A. Gharsallaoui, *Appl. Sci.*, 2024, **14**, 2256.
126 H. Chen, X. Guo, J. Li, Z. Liu, Y. Hu, X. Tao, S. Song and B. Zhu, *Int. J. Biol. Macromol.*, 2023, **242**, 124788.
127 W. Zhang and W. Jiang, *Int. J. Biol. Macromol.*, 2020, **155**, 1252–1261.
128 S. Roy, S. Shankar and J. W. Rhim, *Food Hydrocolloids*, 2019, **88**, 237–246.
129 A. Kalia, M. Kaur, A. Shami, S. K. Jawandha, M. A. Alghuthaymi, A. Thakur and K. A. Abd-Elsalam, *Biomolecules*, 2021, **11**, 224.
130 D. V. Francis, S. Thaliyakattil, L. Cherian, N. Sood and T. Gokhale, *Polymers*, 2022, **14**, 1379.
131 M. Gundhavi Devi and S. Arun Karthick, *Polym. Eng. Sci.*, 2024, **64**, 4128–4143.
132 S. A. Khalil, A. Awadallah-F, M. R. Khaffaga, R. M. Fathy and A. S. Kodous, *Sci. Rep.*, 2024, **14**, 1–16.
133 J. Hanif, N. Khalid, R. S. Khan, M. F. Bhatti, M. Q. Hayat, M. Ismail, S. Andleeb, Q. Mansoor, F. Khan and F. Amin, *Mater. Sci. Eng., C*, 2019, **100**, 82–93.
134 S. Tharani, D. Bharathi and R. Ranjithkumar, *Biocatal. Agric. Biotechnol.*, 2020, **30**, 101838.
135 M. S. Samuel, M. Ravikumar, A. John, E. Selvarajan, H. Patel, P. S. Chander, J. Soundarya, S. Vuppala, R. Balaji and N. Chandrasekar, *Catalysts*, 2022, **12**, 459.
136 C. Hano and B. H. Abbasi, *Biomolecules*, 2022, **12**, 31.
137 N. S. Alharbi, N. S. Alsubhi and A. I. Felimban, *J. Radiat. Res. Appl. Sci.*, 2022, **15**, 109–124.
138 P. K. Dikshit, J. Kumar, A. K. Das, S. Sadhu, S. Sharma, S. Singh, P. K. Gupta and B. S. Kim, *Catalysts*, 2021, **11**, 902.
139 M. S. Akhter, M. A. Rahman, R. K. Ripon, M. Mubarak, M. Akter, S. Mahbub, F. Al Mamun and M. T. Sikder, *Heliyon*, 2024, **10**(11), e29766.
140 M. Fahim, A. Shahzaib, N. Nishat, A. Jahan, T. A. Bhat and A. Inam, *JCIS Open*, 2024, **16**, 100125.
141 S. Talebian, B. Shahnavaz, M. Nejabat, Y. Abolhassani and F. B. Rassouli, *Front. Bioeng. Biotechnol.*, 2023, **11**, 1140010.
142 F. M. Elkady, B. M. Badr, E. Saied, A. H. Hashem, M. S. Abdulrahman, M. M. Alkherkhisy, T. A. Selim, F. M. Alshabrmi, E. A. Alatawi and F. F. Aba Alkhayl, *Sci. Rep.*, 2025, **15**, 18772.
143 D. N. Mishra, L. Prasad and U. Suyal, *Front. Microbiol.*, 2025, **16**, 1506695.
144 M. J. Javid-Naderi, Z. Sabouri, A. Jalili, H. Zarrinfar, S. Sammak and M. Darroudi, *Environ. Technol. Innovation*, 2025, **38**, 104147.
145 D. Singh, D. Jain, D. Rajpurohit, G. Jat, H. S. Kushwaha, A. Singh, S. R. Mohanty, M. K. Al-Sadoon, W. Zaman and S. K. Upadhyay, *Front. Chem.*, 2023, **11**, 1154128.
146 M. F. Baran, C. Keskin, A. Baran, A. Hatipoğlu, M. Yildiztekin, S. Küçükaydin, K. Kurt, H. Hoşgören, M. M. R. Sarker, A. Sufianov, O. Beylerli, R. Khalilov and A. Eftekhari, *Molecules*, 2023, **28**, 2310.
147 C. Santschi, N. Von Moos, V. B. Koman, V. I. Slaveykova, P. Bowen and O. J. Martin, *J. Nanobiotechnol.*, 2017, **15**, 19.
148 L. Pezzi, A. Pane, F. Annesi, M. A. Losso, A. Guglielmelli, C. Umeton and L. De Sio, *Materials*, 2019, **12**, 1078.
149 Y.-N. Gao, Y. Wang, T.-N. Yue, Y.-X. Weng and M. Wang, *J. Colloid Interface Sci.*, 2021, **582**, 112–123.
150 A. Farooq, U. A. Khan, H. Ali, M. Sathish, S. A. H. Naqvi, S. Iqbal, H. Ali, I. Mubeen, M. B. Amir, W. F. A. Mosa, A. Baazeem, M. Moustafa, S. Alrumman, A. Shati and S. Negm, *Microorganisms*, 2022, **10**, 2195.
151 S. El-Sonbaty, E. I. Kandil and R. A.-H. Haroun, *Biol. Trace Elem. Res.*, 2023, **201**, 272–281.
152 S. Ayadi Hassan, P. Ghadam and A. Abdi Ali, *Bioprocess Biosyst. Eng.*, 2022, **45**, 605–618.
153 N. Jayarambabu, A. Akshaykranth, T. Venkatappa Rao, K. Venkateswara Rao and R. Rakesh Kumar, *Mater. Lett.*, 2020, **259**, 126813.
154 V. Paramasivam, P. Paulpandian, K. Venkatachalam, S. Hussain, A. Kangal, D. A. Al Farraj, M. S. Elshikh and P. Balaji, *J. King Saud Univ., Sci.*, 2023, **35**, 102687.
155 M. Horie and Y. Tabei, *Free Radical Res.*, 2021, **55**, 331–342.
156 P. Nie, Y. Zhao and H. Xu, *Ecotoxicol. Environ. Saf.*, 2023, **253**, 114636.
157 S. Medici, M. Peana, A. Pelucelli and M. A. Zoroddu, *Semin. Cancer Biol.*, 2021, **76**, 17–26.
158 D. Dotto, M. Scatolini, S. Pugini, L. Vercik, M. Melo, A. Vercik and E. Rigo, *Mater. Res. Express*, 2021, **8**, 115402.
159 M. S. Mondal, A. Paul and M. Rhaman, *Sci. Rep.*, 2023, **13**, 1–15.
160 K. Santiago-Castillo, A. M. Torres-Huerta, D. Del Ángel-López, M. A. Domínguez-Crespo, H. Dorantes-Rosales, D. Palma-Ramírez and H. Willcock, *Polymers*, 2022, **14**, 674.
161 R. Ahmad and K. Ansari, *Int. J. Biol. Macromol.*, 2022, **218**, 157–167.
162 N. Mohamed and N. G. Madian, *Mater. Today Commun.*, 2020, **25**, 101372.
163 S. Shankar, D. Khodaei and M. Lacroix, *Food Hydrocolloids*, 2021, **117**, 106750.
164 S. Li, B. Gu, X. Li, S. Tang, L. Zheng, E. Ruiz-Hitzky, Z. Sun, C. Xu and X. Wang, *Adv. Healthcare Mater.*, 2022, **11**, 2102367.
165 A. Mamman and P. Jain, *Nano-Struct. Nano-Objects*, 2024, **39**, 101297.

166 S. Ediyilyam, B. George, S. S. Shankar, T. T. Dennis, S. Wacławek, M. Černík and V. V. Padil, *Polymers*, 2021, **13**, 1680.
167 A. Mamman and P. Jain, *Nano-Struct. Nano-Objects*, 2024, **39**, 101297.
168 S. Gunalan, R. Sivaraj and V. Rajendran, *Prog. Nat. Sci.:Mater. Int.*, 2012, **22**, 693–700.
169 M. Hussain Beevi, S. Vignesh, T. Pandiyarajan, P. Jegatheesan, R. Arthur James, N. V. Giridharan and B. Karthikeyan, *Adv. Mater. Res.*, 2012, **488–489**, 666–670.
170 M. H. A. Begum, M. M. Hossain, M. A. Gafur, A. N. M. H. Kabir, N. I. Tanvir and M. R. Molla, *SN Appl. Sci.*, 2019, **1**, 1–9.
171 F. Parvin, M. A. Rahman, J. M. M. Islam, M. A. Khan and A. H. M. Saadat, *Adv. Mater. Res.*, 2010, **123–125**, 351–354.
172 X. Y. Zhou, Y. F. Cui, D. M. Jia and D. Xie, *Polym.-Plast. Technol. Eng.*, 2009, **48**, 489–495.
173 N. Peelman, P. Ragaert, B. De Meulenaer, D. Adons, R. Peeters, L. Cardon, F. Van Impe and F. Devlieghere, *Trends Food Sci. Technol.*, 2013, **32**, 128–141.
174 F. Fahma, Sugiarto, T. C. Sunarti, S. M. Indriyani and N. Lisdayana, *Int. J. Polym. Sci.*, 2017, **2017**(1), 2745721.
175 R. Abedi-Firoozjah, N. Chabook, O. Rostami, M. Heydari, A. Kolahdouz-Nasiri, F. Javanmardi, K. Abdolmaleki and A. M. Khaneghah, *Polym. Test.*, 2023, **118**, 107903.
176 X. Luo, J. Li and X. Lin, *Carbohydr. Polym.*, 2012, **90**, 1595–1600.
177 X. Tang and S. Alavi, *Carbohydr. Polym.*, 2011, **85**, 7–16.
178 W. A. W. A. Rahman, L. T. Sin, A. R. Rahmat and A. A. Samad, *Carbohydr. Polym.*, 2010, **81**, 805–810.
179 L.-S. Wang, C.-Y. Wang, C.-H. Yang, C.-L. Hsieh, S.-Y. Chen, C.-Y. Shen, J.-J. Wang and K.-S. Huang, *Int. J. Nanomed.*, 2015, 2685–2696.
180 S. Akmaz, E. Dilaver Adıgüzel, M. Yasar and O. Erguven, *Adv. Mater. Sci. Eng.*, 2013, **2013**, 690918.
181 K.-S. Huang, C.-Y. Wang, C.-H. Yang, A. M. Grumezescu, Y.-S. Lin, C.-P. Kung, I.-Y. Lin, Y.-C. Chang, W.-J. Weng and W.-T. Wang, *Molecules*, 2013, **18**, 5749–5760.
182 N. M. Zain, A. G. Stapley and G. Shama, *Carbohydr. Polym.*, 2014, **112**, 195–202.
183 T. M. Abou Elmaaty, H. Elsisi, G. Elsayad, H. Elhadad and M. R. Plutino, *Polymers*, 2022, **14**, 4273.
184 S. Mehmood, N. Akhtar, M. Arshad, U. Azhar, S. Ullah, T. S. Waris, F. Jabbar, A. Hasan, F. Iqbal, A. A. Chaudhry, I. ur Rehman and M. Yar, *Int. J. Biol. Macromol.*, 2024, **267**, 129256.
185 P. Wang, Y. Wang, Q. Xu, Q. Chen, Y. Zhang and Z. Xu, *Appl. Surf. Sci.*, 2022, **592**, 153314.
186 Y. N. Gao, Y. Wang, T. N. Yue, Y. X. Weng and M. Wang, *J. Colloid Interface Sci.*, 2021, **582**, 112–123.
187 L. A. Aboelmagd, E. Tolba and Z. A. AbdelAziz, *Polym. Bull.*, 2023, **80**, 4229–4243.
188 H. Chen, G. Zhang, W. Zhang and W. Gao, *RSC Adv.*, 2023, **13**, 11450–11456.
189 E. Abd El-Aziz, M. Zayed, A. L. Mohamed and A. G. Hassabo, *Polymers*, 2023, **15**, 3047.
190 A. I. Ribeiro, V. Shvalya, U. Cvelbar, R. Silva, R. Marques-Oliveira, F. Remião, H. P. Felgueiras, J. Padrão and A. Zille, *Polymers*, 2022, **14**, 1138.
191 A. T. Mogharbel, S. F. Ibarhiam, A. M. Alqahtani, R. M. S. Attar, K. F. Alshammari, M. A. Bamaga, S. D. Al-Qahtani and N. M. El-Metwaly, *J. Ind. Eng. Chem.*, 2023, **127**, 356–364.
192 T. Tuesta, A. Castillo-Barzola, H. Linares, G. Ruiz-Pacco, A. M. Baena-Moncada and A. Valderrama-Negrón, *Food Chem.*, 2025, 144589.
193 J. O. Adeyemi and O. A. Fawole, *Biomolecules*, 2023, **13**, 1092.
194 C. Couto and A. Almeida, *Foods*, 2022, **11**, 402.
195 S. C. Boca, M. Potara, A. M. Gabudean, A. Juhem, P. L. Baldeck and S. Astilean, *Cancer Lett.*, 2011, **311**, 131–140.
196 R. Misra, S. Hazra, S. Saleem and S. Nehru, *Med. Oncol.*, 2024, **41**, 132.
197 N. M. Elbaz, L. Ziko, R. Siam and W. Mamdouh, *Sci. Rep.*, 2016, **6**, 1–9.
198 N. S. Capanema, I. C. Carvalho, A. A. Mansur, S. M. Carvalho, A. P. Lage and H. S. Mansur, *ACS Appl. Nano Mater.*, 2019, **2**, 7393–7408.
199 A. Abaza, G. Mahmoud and B. Elsheikh, *J. Pharm. Pharmacol.*, 2018, **6**, 729–741.
200 W. R. Rolim, J. C. Pieretti, D. L. S. Reno, B. A. Lima, M. H. M. Nascimento, F. N. Ambrosio, C. B. Lombello, M. Brocchi, A. C. S. de Souza and A. B. Seabra, *ACS Appl. Mater. Interfaces*, 2019, **11**, 6589–6604.
201 S. Saadi Ahmed and N. Abbass, *Rep. Biochem. Mol. Biol.*, 2024, **13**(3), 405.
202 A. Muñoz-Bonilla, C. Echeverria, Á. Sonseca, M. P. Arrieta and M. Fernández-García, *Materials*, 2019, **12**, 641.
203 A. Altaf, Z. Usmani, A. H. Dar and K. K. Dash, *Discover Food*, 2022, **2**, 1–13.
204 A. Khezerlou, M. Tavassoli, M. Alizadeh Sani, K. Mohammadi, A. Ehsani and D. J. McClements, *Polymers*, 2021, **13**, 4399.
205 M. Taherimehr, H. YousefniaPasha, R. Tabatabaeekoloor and E. Pesaranhajiabbas, *Compr. Rev. Food Sci. Food Saf.*, 2021, **20**, 5321–5344.
206 B. Dhlamini, H. K. Paumo, B. P. Kamdem, L. Katata-Seru and I. Bahadur, *J. Environ. Chem. Eng.*, 2022, **10**, 107729.
207 R. Sreena and A. J. Nathanael, *Materials*, 2023, **16**(6), 2364.
208 M. C. Biswas, B. Jony, P. K. Nandy, R. A. Chowdhury, S. Halder, D. Kumar, S. Ramakrishna, M. Hassan, M. A. Ahsan and M. E. Hoque, *J. Polym. Environ.*, 2022, **30**, 51–74.
209 F. Riaz, I. Rasul, F. Azeem, M. Zubair, H. Nadeem, M. Imran, A. Muzammil, M. Afzal and M. H. Siddique, in *Advances in Bionanocomposites*, ed. B. Sharma, S. Thomas, P. Kumar Bajpai, K. Ghosal and S. Shekhar, Elsevier, 2024, pp. 387–406.
210 S. C. Carroccio, P. Scarfato, E. Bruno, P. Aprea, N. T. Dintcheva and G. Filippone, *J. Clean. Prod.*, 2022, **335**, 130322.

211 H. Zhang, M. Hortal, A. Dobon, M. Jorda-Beneyto and J. M. Bermudez, Selection of Nanomaterial-Based Active Agents for Packaging Application: Using Life Cycle Assessment (LCA) as a Tool, *Packag. Technol. Sci.*, 2017, **30**(9), 575–586.
212 S. Sarkar, K. Gulati and K. M. Poluri, *Green Polymeric Nanocomposites*, 2020, pp. 251–280.
213 D. L. Schrijvers, F. Leroux, V. Verney and M. K. Patel, *Green Chem.*, 2014, **16**, 4969–4984.
214 S. Temizel-Sekeryan and A. L. Hicks, *Resour. Conserv. Recycl.*, 2020, **156**, 104676.
215 D. B. Tripathy and A. Gupta, *J. Reinf. Plast. Compos.*, 2024, DOI: **10.1177/07316844241233162**.
216 R. Shogren, D. Wood, W. Orts and G. Glenn, *Sustain. Prod. Consum.*, 2019, **19**, 194–215.
217 A. Dirpan, A. F. Ainani and M. Djalal, *Polymers*, 2023, **15**, 2781.
218 D. M. Mitrano, S. Motellier, S. Clavaguera and B. Nowack, *Environ. Int.*, 2015, **77**, 132–147.
219 R. Kumar, G. Ghoshal and M. Goyal, *Mater. Sci. Energy Technol.*, 2020, **3**, 672–678.
220 X. Zhang, Y. Liu, H. Yong, Y. Qin, J. Liu and J. Liu, *Food Hydrocolloids*, 2019, **94**, 80–92.
221 V. Soltaninejad and A. Maleki, *J. Photochem. Photobiol., A*, 2021, **404**, 112906.